Magnetic-Confinement Fusion – Plasma Theory:
Tokamak Magnetohydrodynamic Equilibrium and Stability

Lang L. Lao, Yueqiang Liu, and Alan. D. Turnbull
General Atomics, San Diego, 92186 CA. USA
Emails: Lao@Fusion.gat.com, Liuy@Fusion.gat.com, Turnbull@Fusion.gat.com

Synopsis

Magnetohydrodynamics (MHD) provides a useful model to describe the crucial plasma macroscopic equilibrium and stability behaviors in toroidal tokamak devices by considering the plasma as a conducting fluid interacting with a surrounding confining electromagnetic field. MHD is the most basic plasma model, incorporating most large-scale phenomena, including plasma equilibrium and all major instabilities. MHD equations are obtained by taking moments of the Boltzmann equations for different plasma species. They provide a set of comprehensive physics constrains to compute and optimize the equilibrium plasma shape and pressure and current profiles that are critical to its stability and performance. In the ideal case, the equations have special properties that lead to efficient numerical calculation schemes, the most important of which is the ideal MHD energy principle for linear stability against small departures from equilibrium. In a tokamak plasma, equilibrium pressure is mostly destabilizing for MHD modes, whereas equilibrium current is also often a major driving force. Plasma resistivity creates new freedom for a MHD instability to grow, but there are also cases where the plasma resistivity plays a stabilizing role. Equilibrium toroidal flow and/or flow shear can affect MHD instabilities. Principal MHD instabilities include the internal kink mode, sawtooth, fishbone, external kink, resistive wall mode, resistive interchange, tearing and neoclassical tearing modes (NTMs), locked modes, toroidal Alfven eigenmodes (TAEs), and edge localized modes (ELMs). Fast-growing MHD instabilities can lead to an abrupt plasma disruption and termination that can potentially damage the device plasma facing components (PFCs) and in-vessel structures. An important MHD application is to develop robust techniques to mitigate and control MHD instabilities.

Keywords: Magnetohydrodynamics, MHD equilibrium, MHD stability, MHD instabilities, Grad-Shafranov equation, ideal linear stability, energy principle, Troyon limit, tokamak disruption, shattered pellet injection, dispersive pellet injection, disruption prediction and avoidance, disruption mitigation

Glossary

Alfven velocity	Alfven wave travelling velocity
Beta	The ratio of plasma stored energy to confining magnetic energy
DIII-D	Doublet III dee-shaped tokamak
Disruption	Rapid termination of a plasma discharge
EFIT	Equilibrium reconstruction and fitting code
ELM	Edge localized mode
Flow shear	A measure of radial variation of plasma angular flow across magnetic surfaces
H-mode	High confinement mode

ITER	International thermonuclear experimental reactor, an international project constructing tokamak designed to study fusion plasma production in deuterium-tritium plasmas
Magnetic shear	A measure of radial variation of safety factor across magnetic surfaces
Magnetic surface	A surface formed by magnetic-field lines
MHD	Magnetohydrodynamics
Mode rational surface	A magnetic surface where the safety factor has a rational value
RWM	Resistive wall mode
Safety factor	The number of toroidal transits for each poloidal transit when following a magnetic-field line
Sawtooth	A periodic relaxation in the tokamak plasma central region
Tokamak	A donut shaped toroidal confinement device
VDE	Vertical displacement event

Introduction

In magnetic-fusion confinement devices such as tokamaks, to remain confined and produce fusion power, the plasma must be maintained in a force-balance equilibrium state and stable to perturbations around this state. To keep the plasma away from the surrounding vacuum vessel, the expanding hot-plasma pressure force, and the centrifugal force if the plasma is rotating, must be balanced by a counter magnetic force driven by electrical currents flowing in the external coils. As schematically illustrated in Figs. 1(a) and 1(b), a stationary ball sitting in the bottom of a valley represents a stable equilibrium state, whereas the one sitting on the top of a hill represents an unstable equilibrium state.

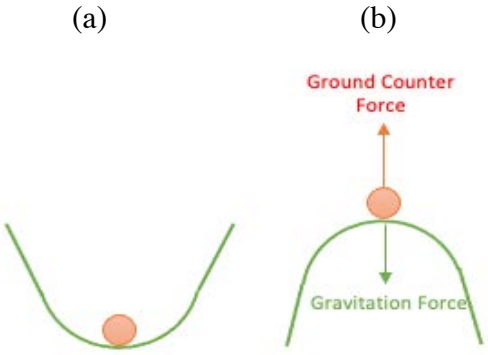

Fig. 1. (a) A stable equilibrium state, (b) an unstable equilibrium state.

Magnetohydrodynamics (MHD) (Bateman 1978, Freidberg 1982) provides a useful model to describe and evaluate this macroscopic plasma equilibrium and stability state by considering the plasma as a conducting fluid confined in a restricted region of space by the electromagnetic force from an externally imposed magnetic field. The magnetic field can be conveniently visualized and represented using magnetic field lines (Boozer 2005). In an axisymmetric toroidal tokamak device,

the magnetic field lines form a set of nested magnetic surfaces in a donut shape. The geometric and topological properties of the magnetic surfaces such as the aspect ratio, elongation, triangularity and squareness play important roles in determining the stability and performance of tokamak plasmas, and can be controlled using a set of external poloidal-field coils.

An important MHD application is to design an optimal set of external poloidal magnetic-field coils to produce a target plasma equilibrium shape that are stable to instabilities. An essential magnetic-fusion research element is to develop the physics basis to support such activities. This requires design and performance of experiments to test the equilibrium and stability properties of the plasma, development and validation of MHD equilibrium and stability physics models to explain the experimental observations, and development of diagnostics and computational tools to accurately measure and efficiently reconstruct the plasma state to interpret the measurements and facilitate the validation.

In an ideal perfectly conducting plasma, the plasma is tied to the magnetic surfaces. In the absence of collisions among ions and electrons and without large drift motions due to magnetic-field gradient and curvature in the magnetic-field lines, the magnetic surfaces act as a container to keep the plasma away from the surrounding vacuum-vessel wall and plasma facing components. The hot plasma pressure and current flowing along the magnetic field lines can act as free-energy sources to drive the plasma away from the desired equilibrium and into various unstable states depending on the particular plasma operating configurations and conditions. The tension and shear in the magnetic-field lines can act as restoring forces to stabilize and keep the plasma in a stable equilibrium state. An excessive amount of plasma stored energy relative to the confining toroidal magnetic field energy or a large amount of flowing plasma current relative to the confining toroidal magnetic-field coil current can drive MHD instabilities that can potentially damage and shorten the lifetime of the confining device PFCs and in-vessel structures.

Two useful physics parameters to describe these important plasma stability properties are the safety factor q and the plasma β. For an axisymmetric toroidal device such as a tokamak, these are defined as

$$q(\psi) = \frac{F(\psi)}{2\pi} \oint_{\psi} \frac{dl_p}{B_p} \frac{1}{R^2} \quad , \tag{1}$$

$$\beta_T = \frac{\int_0^{\Omega_B} P d\Omega}{\Omega_B B_{T0}^2 / 2\mu_0}. \tag{2}$$

Here, B_T and B_P are the toroidal and poloidal component of the magnetic field $\mathbb{B}$ from the electric currents flowing within the plasma plus those flowing in the external toroidal and poloidal magnetic-field coils. $F(\psi) = 2\pi R B_T/\mu_0$ is the poloidal current stream function, R is the plasma major radius, ψ is the poloidal flux per radian of the toroidal angle, and B_{T0} is the vacuum toroidal magnetic field at the geometric center of the plasma boundary surface. The line integration in Eq. (1) is along a poloidal cross section of a magnetic flux surface labeled by ψ, $\Omega(\psi)$ is the volume enclosed by the magnetic surface ψ, and Ω_B is the plasma volume. The safety factor q describes the average pitch of the magnetic field lines along a magnetic surface weighted by the geometric properties of the surface. q represents the number of turns a magnetic field line has to traverse toroidally before completing a poloidal turn.

Additionally, depending on the plasma transport conditions, strong pressure or current gradients can develop locally in a small region near a transport barrier that can act as free-energy source to drive the plasma into an unstable state (Lao 2000). In the tokamak high confinement mode (H-mode) regime (Wagner 2007, Burrell 1987), a large edge pedestal pressure gradient can develop leading to ELMs (Leonard 2014). Large ELMs can shorten the life time of the divertor wall.

MHD is also applied to develop robust techniques to mitigate and control MHD instabilities (Igochine 2015). At high β_T or low q, a small perturbation can lead to unstable plasma motion that strongly distorts the magnetic surfaces allowing the plasma to quickly release its thermal and magnetic energy in a very short time scale, which can potentially damage the plasma-facing components (PFCs) and in-vessel structures. Additionally, at rational q surfaces the magnetic field lines close on themselves rather than spanning the entire surface. A magnetic perturbation that has toroidal and poloidal mode numbers in sync with the pitch of the magnetic field lines can then interact resonantly with the magnetic field and strongly distort the magnetic surfaces, thus allowing the heat flux to quickly transport and escape to the surrounding vacuum-vessel wall. Additionally, together with the plasma resistivity and toroidal asymmetry, magnetic islands and stochastic regions can form around the rational q surfaces within the plasma that can tear open the magnetic surfaces and allow particle and heat flux to also redistribute and escape to the vessel wall. Impurities sputtered from the wall can then enter and accumulate in the plasma and can lead to a radiation induced thermal collapse and rapid decay of the plasma current. The shrinkage of the current channel in the plasma column can make it susceptible to vertical displacement events (VDEs) and then disruption, which can potentially damage the device PFCs and in-vessel structures due to the large attached halo current induced in the surrounding wall (Boozer 2012, Lao 1991, Lehnen 2015, Clauser 2019).

In this Chapter, the physics principles of toroidal tokamak equilibrium and stability are first discussed, including the derivation of the MHD equations from the Boltzmann kinetic equation. This is then followed by a section on toroidal equilibrium including a description of equilibrium reconstruction and the inverse representation. A discussion of MHD stability including linear stability and the energy principle, the effects of plasma resistivity, energetic particles, and plasma toroidal flow is then discussed. A discussion of major MHD instabilities including axisymmetric modes, internal kinks (IKs), resistive-wall modes (RWMs), ELMs, tearing modes (TMs), and TAEs then follows. The plasma response to external 3D magnetic fields and numerical tools to compute MHD instabilities are also described. Lastly, a short discussion of methods and techniques to mitigate and control plasma instabilities including disruptions is given.

Physics principles of toroidal equilibrium and stability

MHD model and equations

MHD is the most basic plasma model, incorporating most large-scale phenomena, including all major instabilities. The model is formally derived from the fundamental Bogoliubov–Born–Green–Kirkwood–Yvon (BBGKY) (Bogoliubov 1946) equations describing an N-body system of N_s charged particles of various species in an electromagnetic field $\mathbb{E}$ and $\mathbb{B}$, coupled with Maxwell's equations for the fields. Each individual particle with (vector) position $\mathbb{x}_n$ and velocity $\mathbb{v}_n$ is acted on by the sum of the Lorentz forces from all other particles of the same or other species

$$m_n \ddot{\mathbb{x}}_n = m_n \dot{\mathbb{v}}_n = \sum_{k \neq n}^{N_s} q_k \left(\mathbb{E} + \mathbb{v}_k \times \mathbb{B}\right). \tag{3}$$

Note that the $\mathbb{x}_k, \mathbb{v}_k$ refer to the particles of various species s; the species label is suppressed here to keep the notation simple. These equations are intractable since $N_s \sim 10^{20}$. A more tractable form is obtained by replacing the full particle distribution function for N_s particles of various species, $F_s(\mathbb{x}_1, \mathbb{v}_1, \mathbb{x}_2, \mathbb{v}_2, \ldots \mathbb{x}_{N_s}, \mathbb{v}_{N_s})$, by a sequence of partial distribution functions, $f_s^{(n)}$, $n = 1,2, \ldots, N_s - 1$, obtained by integrating over the eliminated variables, so that,

$$f_s^{(n-1)}(\mathbb{x}_1, \mathbb{v}_1, \mathbb{x}_2, \mathbb{v}_2, \ldots \mathbb{x}_n, \mathbb{v}_n) \equiv \iint f_s^{(n)}(\mathbb{x}_1, \mathbb{v}_1, \mathbb{x}_2, \mathbb{v}_2, \ldots \mathbb{x}_n, \mathbb{v}_n, \mathbb{x}_{n+1}, \mathbb{v}_{n+1}) d^3\mathbb{x}_{n+1} d^3\mathbb{v}_{n+1}, \quad (4)$$

with $f_s^{(N_s-1)}(\mathbb{x}_1, \mathbb{v}_1, \mathbb{x}_2, \mathbb{v}_2, \ldots \mathbb{x}_{N_s}, \mathbb{v}_{N_s}) \equiv F_s(\mathbb{x}_1, \mathbb{v}_1, \mathbb{x}_2, \mathbb{v}_2, \ldots \mathbb{x}_{N_s}, \mathbb{v}_{N_s})$.

These are the so-called BBGKY equations. These contain similar information as $F_s(\mathbb{x}_1, \mathbb{v}_1, \mathbb{x}_2, \mathbb{v}_2, \ldots \mathbb{x}_{N_s}, \mathbb{v}_{N_s})$, namely the position and velocity of every particle of species s. The final so-called single particle distribution function is then,

$$f_s(\mathbb{x}, \mathbb{v}) \equiv f_s^{(0)}(\mathbb{x}_1, \mathbb{v}_1) = \iint \iint \ldots F_s(\mathbb{x}_1, \mathbb{v}_1, \mathbb{x}_2, \mathbb{v}_2, \ldots \mathbb{x}_{N_s}, \mathbb{v}_{N_s}) \prod_{k=2}^{N_s} (d^3\mathbb{x}_k d^3\mathbb{v}_k). \quad (5)$$

Combining this with the equations of motion for the particles then yields the Boltzmann Equation for $f_s(\mathbb{x}, \mathbb{v})$ (Colonna 2016):

$$\frac{\partial f_s}{\partial t} + \mathbb{v} \cdot \nabla_{\mathbb{x}} f_s + {}^{q_s}/_{m_s} [\mathbb{E}(\mathbb{x}, t) + \mathbb{v} \times \mathbb{B}(\mathbb{x}, t)] \cdot \nabla_{\mathbb{v}} f_s = C_s(f_a, f_\beta, f_\gamma, \ldots, f_s, \ldots f_\zeta). \quad (6)$$

Here, $\nabla_{\mathbb{x}} f_s$ means $\nabla_{\mathbb{x}} f_s \equiv \left(\frac{\partial f_s}{\partial X} \quad \frac{\partial f_s}{\partial Y} \quad \frac{\partial f_s}{\partial Z}\right)^T$, and $\nabla_{\mathbb{v}} f_s \equiv \left(\frac{\partial f_s}{\partial V_s^X} \quad \frac{\partial f_s}{\partial V_s^Y} \quad \frac{\partial f_s}{\partial V_s^Z}\right)^T$ (the T represents the transpose). This coupled set of equations for various particle species (α,β,…,…s,…,ζ) describes the evolution of the probability of finding a particle of species s at any given point $(\mathbb{x}, \mathbb{v})$ in phase space at any given time due to electrodynamic and thermodynamic forces. The final term on the right side formally represents the effects of collisions between species, including those of the same species. For a collisionless plasma, $C_s = 0$, and the equation is called the Vlasov Equation (Colonna 2016). Combined with Maxwell's Equations for the fields, the equations give a complete self-consistent account of the system of charged particles.

The MHD equations are obtained by taking velocity moments of the Boltzmann equations, for electrons and each ion species. For the velocity $\mathbb{v} \equiv (V_s^X \quad V_s^Y \quad V_s^Z)^T$, the velocity moments are defined by,

$$< V_s^\alpha V_s^\beta .. V_s^\zeta >_s \equiv {\int V^\alpha V^\beta .. V^\zeta f_s(X,V) d^3\mathbb{v}}/{\int f_s(X,V) d^3\mathbb{v}}, \quad (7)$$

for each of the coordinates, $\alpha, \beta, \ldots, \zeta \in \{X, Y, Z\}$. We will use the notation V_s^α (with the s subscript) when designating the velocity moments. Without the subscript they refer to dummy integration variables. The first velocity moment (zeroth order) is just the number density defined as:

$$n_s(\mathbb{x}) = < n_s > = \int f_s(\mathbb{x}, \mathbb{v}) d^3\mathbb{v}. \quad (8)$$

The second is the species single-fluid velocity, with three different moments corresponding to the three coordinate directions:

$$V_s^\alpha(\mathbb{x}) = < V_s^\alpha > = {\int V^\alpha f_s(\mathbb{x}, \mathbb{v}) d^3\mathbb{v}}/{\int f_s(\mathbb{x}, \mathbb{v}) d^3\mathbb{v}}. \quad (9)$$

The third describes the energy for each species defined as:

$$\frac{1}{2}n_s(\mathbb{x})T_s^{\alpha,\beta}(\mathbb{x}) = \int \frac{1}{2}m_s\left(V^\alpha - V_s^\alpha(\mathbb{x})\right)\left(V^\beta - V_s^\beta(\mathbb{x})\right) f_s(\mathbb{x},\mathbb{v})d^3\mathbb{v}. \quad (10)$$

This is a symmetric tensor and the temperature for each species is then just found from

$$T_s(\mathbb{x}) = [T_s^{x,x}(\mathbb{x}) + T_s^{y,y}(\mathbb{x}) + T_s^{z,z}(\mathbb{x})]/3, \quad (11)$$

$$T_s^{\alpha,\alpha}(\mathbb{x}) = < m_s\left(V^\alpha - V_s^\alpha(\mathbb{x})\right)^2 >_s. \quad (12)$$

A pressure tensor for each species can also be defined. This is a symmetric tensor, $\mathbb{P}$, with components

$$P_s^{\alpha,\beta}(\mathbb{x}) \equiv n_s(\mathbb{x})T_s^{\alpha,\beta}(\mathbb{x}) =< m_s\left(V^\alpha - V_s^\alpha(\mathbb{x})\right)\left(V^\beta - V_s^\beta(\mathbb{x})\right) >_s \int f_s(\mathbb{x},\mathbb{v})d^3\mathbb{v}. \quad (13)$$

The tensor $\mathbb{T}$ and the temperature $T_s(\mathbb{x})$ are in units of energy so $T_s(\mathbb{x})$ is really k times the temperature in Kelvins, where k is the Boltzmann's constant.

The full set of moment equations coupled with Maxwell's equations provides a complete formal description of the system. The first two moments provide a set of equations that essentially describe mass and momentum conservation for each species. For a plasma of just two species, ions and electron, one can recombine these first moment equations into a single-fluid form by replacing each pair of species equations by their weighted sum and difference to eliminate $\mathbb{v}_i$ and $\mathbb{v}_e$ by the fluid velocity $\mathbb{v}$, which is the common velocity of the two species,

$$\mathbb{v} \equiv (m_i n_i \mathbb{v}_i + m_e n_e \mathbb{v}_e)/(m_i n_i + m_e n_e), \quad (14)$$

and the velocity difference represented by the current density,

$$\mathbb{j} = (q_i n_i \mathbb{v}_i + q_e n_e \mathbb{v}_e). \quad (15)$$

The total mass density is,

$$\rho_m = (m_i n_i + m_e n_e), \quad (16)$$

and the total (tensor) pressure is,

$$\mathbb{P} = \mathbb{P}_i + \mathbb{P}_e. \quad (17)$$

Then, the zeroth-order moment becomes the particle conservation equation;

$$\frac{\partial \rho}{\partial t} + \nabla \cdot (\rho \mathbb{v}) = 0, \quad (18)$$

familiar from conventional fluid theory. The first order moment equations become a simple force balance momentum conservation equation, which can be written as the vector equation,

$$\rho\left(\frac{\partial \mathbb{v}}{\partial t} + (\mathbb{v}\cdot\nabla)\mathbb{v}\right) + \nabla \cdot \mathbb{P} - (\mathbb{j} \times \mathbb{B}) = 0. \quad (19)$$

The first two terms on the left represent the inertia. The other two terms are the pressure force and the electromagnetic force. In equilibrium, with $\mathbb{v} = 0$, the pressure and electromagnetic forces are balanced. While at this point the model is two-fluid, these equations are in a single-fluid form.

In general, higher velocity moments from higher order equations are required in each new equation, and at second order, the situation becomes significantly more complicated. The individual electron and ion terms cannot be completely eliminated without additional approximations. At second order, one obtains two equations. One is effectively a generalized Ohm's Law

$$\mathbb{E} + \mathbb{v} \times \mathbb{B} = \eta \mathbb{j} + \mathbb{R}. \tag{20}$$

$$\mathbb{R} = \left({}^{1}/_{q_e n_e}\right)\nabla \cdot \mathbb{P}_i + \left({}^{\Delta n_e}/_{n_e}\right)\mathbb{E} + \left({}^{m_i}/_{q_i}\right)\left(\frac{\partial \mathbb{v}}{\partial t} + (\mathbb{v} \cdot \nabla)\mathbb{v}\right) + \left({}^{m_e}/_{q_e}\right)\left(\frac{\partial(\mathbb{v}_i - \mathbb{v}_e)}{\partial t} + (\mathbb{v} \cdot \nabla)(\mathbb{v}_i - \mathbb{v}_e)\right). \tag{21}$$

$\mathbb{R}$ contains the remaining unbalanced two-fluid terms, including the Hall effect. Most are small and can normally be neglected. The other is a tensor equation for the evolution of the pressure tensor, $\mathbb{P}$ given below.

Truncating the separate ion and electron equations at this order, then one obtains the full set of MHD equations:

$$\frac{\partial \rho}{\partial t} + \nabla \cdot (\rho \mathbb{v}) = 0, \tag{22}$$

$$\frac{\partial \sigma}{\partial t} + \nabla \cdot \mathbb{j} = 0, \tag{23}$$

$$\frac{\partial \mathbb{B}}{\partial t} + \nabla \times (\mathbb{E}) = 0, \tag{24}$$

$$-\frac{1}{c^2}\frac{\partial \mathbb{E}}{\partial t} + \nabla \times (\mathbb{B}) = \mu_0 \mathbb{j}, \tag{25}$$

$$\nabla \cdot \mathbb{B} = 0, \tag{26}$$

$$\nabla \cdot \mathbb{E} = \epsilon_0^{-1}\sigma\ , \tag{27}$$

$$\rho\left(\frac{\partial \mathbb{v}}{\partial t} + (\mathbb{v} \cdot \nabla)\mathbb{v}\right) = \sigma\mathbb{E} + \mathbb{j} \times \mathbb{B} - \nabla \cdot \mathbb{P}, \tag{28}$$

$$\mathbb{E} + \mathbb{v} \times \mathbb{B} = \eta \mathbb{j} + \mathbb{R}. \tag{29}$$

$$\frac{\partial}{\partial t}\mathbb{P} + (\mathbb{v} \cdot \nabla)\mathbb{P} = \nabla \cdot \mathbb{T} + \mathbb{q}, \tag{30}$$

with $\mathbb{T}$ representing a (generalized) stress-energy tensor and $\mathbb{q}$ an energy (heat) flux. In this general form, MHD is a full two-fluid theory but it is not closed. The stress-energy tensor and energy flux in Eq. (30), are obtained formally from the higher order truncated terms but most closures involve specifying them independently instead, along with several simplifying assumptions for $\mathbb{R}$.

Various closure schemes are possible and these lead to different versions of MHD. The most important approximation is the Darwin Approximation;

$$\frac{1}{c^2}\frac{\partial \mathbb{E}}{\partial t} \ll \nabla \times \mathbb{B} \sim \mu_0 \mathbb{j}, \tag{31}$$

which essentially eliminates propagating purely electromagnetic waves from the system. This is almost always a good approximation and is consistent with the ignoring of relativistic dynamics. Of the various simplified MHD models, the Darwin approximation is the most valid and is almost

always assumed. With the Darwin approximation, the remaining equations are usually referred to as the 'Two-Fluid MHD Equations", or sometimes, with an appropriate closure, as the Extended MHD Equations.

The remaining common assumptions such as no resistivity $\eta = 0$, isotropic pressure $p_\perp = p_\parallel$, or $T_e = T_i$ are variously valid under different circumstances. These are usually based on approximations from fluid dynamics and thermodynamics. For example, relations between $\mathbb{P}$ and the mass density for each species, or an assumption for off-diagonal pressure (stress) terms in $\mathbb{P}$ are often used. Separate leftover electron terms of the full two-fluid model (Hall and ∇p_e terms) are commonly dropped as small leaving simpler single-fluid equations. These are usually referred to as 'the MHD Equations' or the 'Single-Fluid MHD' equations. Assuming a scalar pressure, one obtains a much simpler system with relatively simple closure options. An alternative is the Chew-Goldberger-Low CGL model (Hunana 2019) which allows for pressure anisotropy $P_\perp \neq P_\parallel$. Finally, if the resistivity is also ignored, $\eta\mathbb{j} \ll \mathbb{v} \times \mathbb{B} \sim \mathbb{E}$, then $\mathbb{E} + \mathbb{v} \times \mathbb{B} \sim 0$ and

$$\frac{\partial \mathbb{B}}{\partial t} = \nabla \times (\mathbb{v} \times \mathbb{B}), \tag{32}$$

implies that the fluid moves with the fields; there is no slippage between them. This condition is called the frozen flux theorem and the resulting MHD model is commonly referred to as 'ideal MHD'. In addition, since the equations are physically intuitive, representing various conservation laws, ad-hoc phenomenological terms can be included as closures to model effects that have been eliminated, for example, fast-particle drive effects, or neoclassical effects.

Toroidal equilibrium

The shape of the equilibrium magnetic surfaces plays an important role in determining its stability and performance. The ideal MHD momentum balance Eq. (19) provides a comprehensive physics constraint to compute and optimize the required external poloidal magnetic-field coil set and its currents necessary to produce a target plasma boundary shape (defined as the largest closed magnetic surface enclosed by the surrounding limiter and vacuum vessel), and the diversion of the external magnetic-field lines to direct the particle and heat flux to the divertor collecting plate.

At equilibrium and in the absence of plasma flow and pressure anisotropy, the MHD equilibrium Eq. (19) and Ampere's law Eq. (25) become

$$\nabla P = \mathbb{j} \times \mathbb{B}, \tag{33}$$

$$\nabla \times \mathbb{B} = \mu_0 \mathbb{j}. \tag{34}$$

It follows from Eqs. (33) and (34) that the confining magnetic force is in the direction perpendicular to the magnetic field lines. At equilibrium, the pressure must be constant on a magnetic flux surface $P = P(\psi)$ and the plasma current density $\mathbb{j}$ flows along the surface.

In a toroidal axisymmetric device such as tokamak, a set of 2D nested magnetic surfaces is formed using a toroidal-field and a poloidal-field coil set. A dedicated Ohmic-coil set is also sometimes employed to drive the toroidal current flowing within the plasma to ease control as in the DIII-D (Luxon 2002) and ASDEX Upgrade (Gruber 1986) tokamaks, rather than combining the functionality into a single set of poloidal-field coils for both shaping and driving Ohmic current as in more recent superconducting long-pulse tokamak devices such as EAST (Wan 2006), KSTAR

(Lee 1999), JT-60SA (Kamada 2011), and ITER[1] (ITER Physics Basis Editors 1999a). In the presence of toroidal asymmetry, magnetic islands and stochastic regions can form that can degrade the plasma confinement and make it more susceptible to MHD instabilities.

Axisymmetric 2D Grad-Shafranov equilibrium

In an axisymmetric toroidal device such as a tokamak, Eqs. (33) and (34) can be combined to yield a 2D elliptic equilibrium equation, the Grad-Shafranov (GS) equation (Grad 1956, Shafranov 1958), by considering force balance in the direction perpendicular to the magnetic field $\mathbb{B}$ and using a cylindrical (R, φ, Z) coordinate system centered at the symmetric axis and dropping the toroidal φ-dependent terms

$$\Delta^* \psi = -\mu_0 R j_\varphi(R, \psi), \tag{35}$$

$$j_\varphi = RP'(\psi) + \frac{\mu_0 FF\prime(\psi)}{4\pi^2 R}. \tag{36}$$

Here, the operator $\Delta^* = R^2 \nabla . (\nabla / R^2)$. The magnetic field can be conveniently represented as

$$\mathbb{B} = \frac{\mu_0 F(\psi)}{2\pi} \nabla\varphi + \nabla\psi \times \nabla\varphi. \tag{37}$$

The first term in Eq. (37) represents the toroidal component of $\mathbb{B}$, whereas the second term represents the poloidal component.

The GS equilibrium, Eq. (35), is based on the cylindrical (R, φ, Z) coordinate system. An alternative coordinate system is the inverse magnetic-flux coordinate system (ρ, θ, φ) using a flux-surface label $\rho(\psi)$ and a poloidal angle θ as independent variables (Boozer, 2005). The GS Eq. (35) can then be transformed to become the inverse GS equation for $R(\rho, \theta)$ or $Z(\rho, \theta)$ (Lao 1981). Since the pressure $P(\psi)$ is constant on a flux surface, the inverse magnetic-flux coordinate system (ρ, θ, φ) provides a particularly convenient coordinate system to study plasma equilibrium, transport, and stability physics. In the case of a diverted plasma, the use of the magnetic-flux coordinate system is restricted to the nested magnetic-surface region within the plasma to avoid the singularity at the separatrix surface that appears in the Jacobian for transformation from the (R, φ, Z) to the (ρ, θ, φ) coordinate system.

Equation (35) represents a differential form of the GS equation. It acts as a constraint linking the derivatives of ψ to the current sources. Given two stream functions describing the toroidal current density source such as $P(\psi)$ and $F(\psi)$ as shown in Eq. (36) and appropriate boundary conditions, Eq. (35) can be solved for the poloidal flux function ψ. Two other forms of the GS Eq. (35) useful for finding equilibrium solutions are the integral and the variational Lagrangian form (Grad 1956, Lao 1981, Lao 1985a, Lao 2005)

$$\psi(\mathbb{x}) = \sum_j G_\psi(\mathbb{x}, \mathbb{x}') I_{ej} + \int_{\Omega_B} G_\psi(\mathbb{x}, \mathbb{x}') j_\varphi [R', \psi(\mathbb{x}')], \tag{38}$$

$$W = \int_{\Omega_B} \left(\frac{B_P^2}{2\mu_0} - \frac{B_T^2}{2\mu_0} - P\right) d\Omega. \tag{39}$$

Here $G_\psi(\mathbb{x}, \mathbb{x}')$ is the Green induction function relating $\psi(\mathbb{x})$ to the current source at $\mathbb{x}'$. The variation Lagrangian form Eq. (39) provides a systematic mean to transform the solution $\psi(R, Z)$

[1] https://www.iter.org/

of the 2D GS equilibrium Eq. (35) into a series of 1D moment equations for the Fourier amplitudes of $R(\rho,\theta)$ or $Z(\rho,\theta)$ (Lao, 1981). The 2D variational moment approach has been successfully generalized to provide a robust and efficient method to find equilibrium solutions in 3D toroidal geometry with nested magnetic surfaces (Bhattacharjee 1983, Hirshman 1983, Lao 1985c).

Analytical solutions exist when the current source Eq. (36) has simple forms (Solovev 1968, Srinivasan 2010) or when the magnetic surface has simple circular geometry (Lao 1981). In general, the GS Eq. (35) or its integral or variation form Eq. (38) or (39) must be solved numerically (Johnson 1979, Takeda 1991). Many tools are available to numerically search and compute the equilibrium solutions given two stream functions describing the toroidal current density source and appropriate boundary conditions (Lao 1984, Lao 1985a, Haney 1995, Ivanov 2009). One class of applications is to find a solution that best matches a specified target plasma boundary given the two stream functions, a set of external poloidal-field coils, and a surrounding limiter. An example of a DIII-D equilibrium computed with the EFIT code (Lao 1985a) is given in Fig. 2. Another class of applications is to find a solution that best matches a specified target plasma boundary but with the two stream functions self-consistently computed based on the plasma transport properties (Grad 1970, Hirshman 1979, Meneghini 2016).

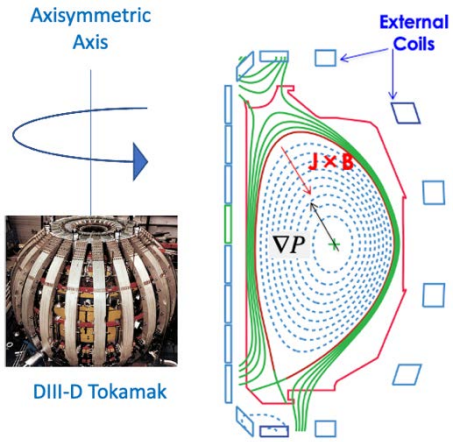

Fig. 2. Poloidal cross-section of a DIII-D tokamak lower single-null equilibrium computed using the EFIT equilibrium code. Also shown is a photo of the DIII-D tokamak with its toroidal- and poloidal-field coils.

Equilibrium Reconstruction

Reconstruction of experimental MHD equilibria is fundamental to tokamak research and operation and is an important part of fusion data analysis and plasma control. Equilibrium reconstruction provides essential magnetic geometry and current and pressure profiles information necessary to support tokamak operation and data analysis, and has contributed to several major physics discoveries, such as the experimental validation of theoretically predicted β stability limits (Strait 1994a) and the negative central-shear operating regime (Levinton 1995, Strait 1995).

A particular important application of the GS Eq. (35) is to reconstruct the experimental plasma equilibrium from various available measurements such as external magnetic and internal current and kinetic profile diagnostics (Lao 1985a, Lao 1990, Lao 2005.) The amount of plasma

information that can be reconstructed increases with the availability of the measurements. External magnetic measurements alone can only yield the plasma boundary shape and global plasma pressure and current profile parameters, such as poloidal β , $\beta_P = \int_0^{\Omega_B} P d\Omega / (\Omega_B B_{PA}^2 / 2\mu_0)$, and internal inductance of the plasma current density profile $\ell_i = \int_0^{\Omega_B} B_P^2 d\Omega / (\Omega_B B_{PA}^2)$, and $B_{PA} = \oint_{\psi_B} B_P \, dl_p / \oint_{\psi_B} dl_p$ is the average poloidal magnetic field along the plasma boundary surface (Lao 1985b, Braams 1991). For critical applications such as analysis and control of MHD instabilities that require detailed pressure and current profile information, accurate full equilibrium reconstruction with kinetic and internal current profiles in addition to external magnetic measurements is required, as well as high spatial-resolution and tightly converged equilibrium solutions (Lao 1990, Ren 2011). Plasma control also imposes a stringent requirement on the equilibrium reconstruction computational speed. Various efficient numerical algorithms and high-performance computation technology have been developed and employed to reconstruct tokamak experimental equilibria in real time to provide the information necessary for plasma control (Ferron 1998, Moret 2015, Rampp 2017, Huang 2020).

MHD stability

Introduction and overview

In principle, the full nonlinear (Extended) MHD model should be reliable under the conditions that the plasma be quasi-neutral and that the length and time scales be long: specifically that the length scales be of the order of the plasma minor radius, and much larger than microscopic scales like the Larmor radius, and that the time scales are much slower than Alfvenic times.

Experimental diagnostic capabilities have been developed to the point where detailed predictions from MHD theory can be productively tested. As discussed in the previous Equilibrium Reconstruction Section, the key to this development has been the progress in reconstructing equilibria obeying MHD force balance and consistent with experimentally measured kinetic profiles (Lao 1990). The linear MHD stability predictions using high quality discharge full equilibrium reconstructions have been thoroughly tested against observations for the principal limiting phenomena and MHD generally predicts ideal current and pressure limits well (Turnbull 2002, Turnbull 2005). In particular, global pressure driven instabilities are predicted to be unstable when the plasma β_T exceeds a value typically of a few percent. β_T measures the amount of thermal energy the plasma can hold for a given magnetic field strength.

A series of numerical ideal MHD stability calculations in the mid 1980's discovered that the limiting β_T obeys a scaling known as the Troyon limit, given originally as

$$\beta_T \leq \beta_{TROY} \equiv C_T \ (\mu_0 I_P) \ / \ (aB_T), \qquad (40)$$

where C_T=2.8 if I_P is in Amperes and B_T is in Tesla (Troyon 1984). This was immediately confirmed by experiments on a number of tokamaks (Stambaugh 1984) and is commonly referred to as the Troyon beta limit[2]

$$\beta_T \leq \ \beta_N^{max} I_P(\mathrm{MA}) \ / \ (aB_T), \qquad (41)$$

[2] This has been a point of confusion; the difference between C_T and β_N^{max} has erroneously been claimed to be a discrepancy.

with β_N^{max}= 3.5. In subsequent years, the Troyon limit scaling has been modified to account for the major profile and shaping effects. The most recent version replaces a constant β_N^{max}= 3.5 by

$$\beta_N^{max} = k_\beta \ell_i \tag{42}$$

where ℓ_i is the internal inductance of the current density profile and k_β varies from 2.5 for conventional elongated, single null, low-triangularity plasmas to $k_\beta = 4$ for high-triangularity double-null plasmas. In spherical tokamaks, the value can be much higher (Sabbagh 2006). The ℓ_i dependence is consistent with results from an analytical ideal ballooning β-limit study (Lao 1992), and a numerical study of the *n*=1 ideal kink β-limit (Howl 1992).

Ideal linear MHD stability and Energy Principle

In the ideal case, the equations have special properties that lead to efficient numerical calculation schemes, the most important of which is the ideal MHD energy principle for linear stability against small departures from equilibrium. Assuming an ideal equilibrium without flows $\mathbb{v}_0 = 0$ and a scalar pressure, the dynamic quantities can be linearized in the small perturbation: $P(\mathbb{x}, t) = P_0(\mathbb{x}) + P(\mathbb{x}, t)$; $\mathbb{j}(\mathbb{x}, t) = \mathbb{j}_0(\mathbb{x}) + \mathbb{j}_1(\mathbb{x}, t)$; and $\mathbb{B}(\mathbb{x}, t) = \mathbb{B}_0(\mathbb{x}) + \mathbb{B}_1(\mathbb{x}, t)$, with each perturbed quantity assumed much smaller than the equilibrium term, yielding an equation for the equilibrium and an equation describing the linear first-order force balance

$$\nabla P_0 = \mathbb{j}_0 \times \mathbb{B}_0 = \left(1/\mu_0\right)(\nabla \times \mathbb{B}_0) \times \mathbb{B}_0, \tag{43}$$

$$\rho_0 \left(\frac{\partial \mathbb{v}_1}{\partial t}\right) + \nabla P_1 = \mathbb{j}_1 \times \mathbb{B}_0 + \mathbb{j}_0 \times \mathbb{B}_1. \tag{44}$$

From here, in order to simplify the subsequent notation, we write $\mathbb{B} = \mathbb{B}_0$, and $\delta\mathbb{B}_p = \mathbb{B}_1$ and similarly for $\mathbb{j} = \mathbb{j}_0$ and $\delta\mathbb{j}_p = \mathbb{j}_1$. The ideal MHD frozen flux relation becomes a relation between the perturbed field $\delta\mathbb{B}_p$ and fluid displacement ξ;

$$\delta\mathbb{B}_p = \nabla \times (\xi \times \mathbb{B}). \tag{45}$$

$\xi \times \mathbb{B}$ is the perturbed vector potential. After some algebra, one finds an equation of motion for the small displacement $\xi(\mathbb{x}, t)$ and perturbed velocity $\mathbb{v}_1(\mathbb{x}, t) \equiv \dot{\xi}(\mathbb{x}, t)$;

$$\rho_0 \ddot{\xi}(\mathbb{x}, t) = \mathfrak{F}\big(\xi(\mathbb{x}, t)\big), \tag{46}$$

with $\mathfrak{F}(\xi)$ a linear operator on ξ: $\mathfrak{F}(\xi) \equiv \mathbb{F}(\mathbb{x}) \cdot \xi$;

$$\mathfrak{F}(\xi) \equiv \mathbb{F}(\mathbb{x}) \cdot \xi \equiv \left(\frac{1}{\mu_0}\right)\left[\left(\left(\nabla \times \delta\mathbb{B}_p\right) \times \mathbb{B}\right) + \left((\nabla \times \mathbb{B}) \times \delta\mathbb{B}_p\right)\right] + \nabla(\xi \cdot \nabla P + \gamma P \nabla \cdot \xi). \tag{47}$$

$\mathbb{F}(\mathbb{x})$ is known as the (linearized) force operator. The solutions to $\xi(\mathbb{x}, t)$ must be temporally exponential, $\xi(\mathbb{x}, t) \equiv \xi(\mathbb{x})e^{i\omega t}$, leading to an eigenvalue equation for the spatial variation of the displacement, $\xi(\mathbb{x})$ and its eigenvalue ω^2;

$$\rho_0^{-1}\mathbb{F}(\mathbb{x}) \cdot \xi(\mathbb{x}) = -\omega^2 \xi(\mathbb{x}). \tag{48}$$

Note that $\xi^\dagger \cdot \mathbb{F} \cdot \xi = \mathfrak{F}(\xi) \cdot \xi^\dagger$ represents the work done by the infinitesimal force $\mathfrak{F}(\xi)$ against the infinitesimal displacement ξ.

Boundary conditions need to be applied by specifying the displacement of the plasma boundary. For a plasma surrounded by a vacuum region and possibly a conducting wall outside, this is not

explicitly known. Boundary conditions can be set, however, by solving simultaneously for $\delta\mathbb{B}_p$ and $\xi(\mathbb{x})$ and the ideal frozen flux relation linking them, and solving for the perturbed vacuum field, $\delta\mathbb{B}_v$, in the annulus between the plasma and the wall.

$$\nabla \times \delta\mathbb{B}_v = \nabla \cdot \mathbb{B}_v = 0, \tag{49}$$

which is most easily solved in terms of a magnetic potential, $\delta\mathbb{B}_v = \nabla\Phi$;

$$\nabla^2\Phi = 0. \tag{50}$$

An appropriate magnetic boundary condition for a conducting wall, or for a wall at infinity can then be applied;

$$\hat{\mathbb{m}} \cdot \nabla\Phi|_w = 0. \tag{51}$$

The perturbed fields must then be matched across the plasma boundary. This condition is complicated since they must be matched across the perturbed boundary;

$$\hat{\mathbb{m}} \cdot \delta\mathbb{B}_p\big|_{pv} = \hat{\mathbb{m}} \cdot \nabla\Phi|_{pv}. \tag{52}$$

The matrix $\mathbb{F}(\mathbb{x})$ is self-adjoint (or Hermitian); $\xi^\dagger \cdot \mathbb{F} \cdot \xi = \xi \cdot \mathbb{F} \cdot \xi^\dagger$.

The Hermitian property provides a number of computational advantages (Bernstein 1957). Notably, the eigenvalues $-\omega^2$ are purely real. Thus, the solutions are either purely growing or damped or are purely oscillatory. The Hermitian property also means one can conveniently reformulate the dynamic problem as a variational problem. Pre-multiplying the equation of motion in the plasma by the adjoint, $\xi^\dagger$, and integrating over all space, one obtains a variational principle (Bernstein 1957). Application of physically relevant boundary conditions in the variational formulation is non-trivial. This is solved by deriving an extended form of the energy principle in which conditions across the plasma vacuum interface, Eq. (52), above are automatically satisfied by the variational solutions. Formulated as a statement of conservation of energy, the extended form of the energy principle is;

$$\delta W - \omega^2 \delta K = 0, \tag{53}$$

$$\delta W\left(\xi, \xi^\dagger, \delta\mathbb{B}_v, \delta\mathbb{B}_v{}^\dagger\right) \equiv \delta W_p\left(\xi, \xi^\dagger\right) + \delta W_v\left(\delta\mathbb{B}_v, \delta\mathbb{B}_v{}^\dagger\right), \tag{54}$$

$$\delta K\left(\xi, \xi^\dagger\right) \equiv {}^1\!/_2 \int_p \rho_0(\mathbb{x}) \left(\xi^\dagger \cdot \xi\right) d^3\mathbb{x}, \tag{55}$$

$$\delta W_p\left(\xi, \xi^\dagger\right) \equiv {}^1\!/_{2\mu_0} \int_p \left(\xi^\dagger \cdot \mathbb{F}(\mathbb{x}) \cdot \xi\right) d^3\mathbb{x}, \tag{56}$$

$$\delta W_v\left(\delta\mathbb{B}_v, \delta\mathbb{B}_v{}^\dagger\right) \equiv {}^1\!/_{2\mu_0} \int_p \left(\delta\mathbb{B}_v{}^\dagger \cdot \delta\mathbb{B}_v\right) d^3\mathbb{x}. \tag{57}$$

δW_v is the vacuum energy contribution from perturbing the plasma boundary. The integrals δK and δW_p are over the plasma volume, and δW_v is over the annular vacuum region. δW represents the total potential energy and δK is the kinetic energy of the perturbing motion. Then δW_p is the plasma potential energy. The energy principle states that if a physically permissible displacement ξ can be found such that $\delta W\left(\xi, \xi^\dagger\right) > 0$, then the plasma is unstable. The energy principle can therefore be used in a trial function approach. Finding a physically permissible trial function, ξ_0, for which $\delta W\left(\xi_0, \xi_0^\dagger\right) > 0$, thus guarantees instability. Note, however, that the trial function is not

necessarily the instability that would appear. The variational principle only implies that this or another more unstable mode will be destabilized.

Substituting for $\mathbb{F}(\mathbb{x})$, the Extended MHD Principle potential energy becomes after some algebra:

$$\delta W_p = \frac{1}{2}\iiint \left[{\delta \mathbb{B}_p^2}/{\mu_0} - \xi_\perp^* \cdot \left(\mathbb{j} \times \delta \mathbb{B}_p\right) + (\xi_\perp . \nabla P)\nabla \cdot \xi_\perp^* + \gamma P |\nabla \cdot \xi|^2 \right] d^3\mathbb{x} \,. \qquad (58)$$

The integral in δW_p is over the plasma and the condition applied is simply that $\delta \mathbb{B}_p = \delta \mathbb{B}_v$ at the plasma vacuum interface. The terms in δW_p can be interpreted physically. The first term in δW_p represents the energy required to bend the field lines. It is always stabilizing – it takes energy input to create this; it is the energy in the perturbed field. The second term, $\xi_\perp^* \cdot \left(\mathbb{j} \times \delta \mathbb{B}_p\right)$ is the destabilization from the current density. The third term is the pressure drive through $\xi_\perp . \nabla P$. The final term represents the energy associated with plasma compression. δW_p can be rewritten in the alternative form;

$$\delta W_p = \frac{1}{2}\iiint \left[{\delta \mathbb{B}_\perp^2}/{\mu_0} + \left({\mathbb{B}^2}/{\mu_0}\right) |\nabla \cdot \xi_\perp + 2\xi_\perp \cdot \kappa|^2 - \left| {\mathbb{j}_\parallel}/{\mathbb{B}} \right| (\xi_\perp^* \times \mathbb{B}) . \delta \mathbb{B}_\perp - 2(\xi_\perp . \nabla P)(\xi_\perp^* \cdot \kappa) + \right.$$
$$\left. \gamma P |\nabla \cdot \xi|^2 \right] d^3\mathbb{x} \,. \qquad (59)$$

This shows more clearly the physical meaning of the terms. The first represents the energy required to bend field lines. The second corresponds to the energy involved in compression of the field. The third and fourth terms are respectively the destabilization from current driven modes, proportional to $|\mathbb{j}_\parallel/\mathbb{B}|$ and ∇P, respectively. The last term, again is the energy from the fluid compression.

The MHD model works extremely well in most situations. In particular, the plasma cross section shape is easily included, at least in numerical calculations as boundary conditions, thus fully capturing the most basic zeroth order effect. MHD is now recognized as an indispensable guide to any design efforts.

Pressure effects

Plasma equilibrium pressure is mostly destabilizing for MHD modes. Associated with the destabilization is the free energy contained in the pressure gradient. This is evident from the ideal MHD energy principle, where the term $-(\xi_\perp \cdot \nabla P)(\xi_\perp^* \cdot \kappa)$ from Eq. (59), integrated over the plasma volume, can be negative and thus provides destabilization. This is the drive term for the ballooning and interchange instabilities. Both the pressure gradient and the global or local value of the pressure amplitude, when exceeding certain critical values, trigger MHD instabilities. Below are important examples. The pressure driven ideal external kink mode becomes unstable when the (global) plasma pressure (often measured in a normalized manner i.e., $\beta_T/[I_p/(aB_T)]$) exceeds the Troyon limit (Troyon 1984)[3]. The ideal internal kink mode becomes unstable when the plasma pressure (often measured in poloidal beta value β_p) exceeds the Bussac limit (Bussac 1975). The infernal mode becomes unstable when β_p exceeds a critical value which linearly scales with Δq, which measures proximity of the global or local q_{min} value to a rational number. The NTM, which is generally a non-linear MHD mode, requires a seed island of finite size which scales with β_p.

[3] Being a global instability, the external kink mode is not sensitive to the local pressure gradient, but is still driven by the "global" pressure gradient which is often measured by the so-called pressure peaking factor.

Besides these direct drives, equilibrium plasma pressure gradient also induces bootstrap optimized[4] which in turn can drive MHD instabilities.

The plasma equilibrium pressure (or pressure gradient) can also be stabilizing for certain MHD modes. The most prominent example is probably the second ballooning stability regime, which is largely due to the large Shafranov shift induced field line compressing at the low-field side of the plasma, where the ballooning mode is typically located due to unfavorable magnetic curvature. In a tokamak plasma, the interchange index D_R can be negative and scales with the local equilibrium pressure gradient at the mode rational surface. This leads to tearing mode stabilization from the favorable average curvature effect (Glasser 1975).

Current effects

Plasma equilibrium current is often a major driving force for MHD instabilities in a tokamak plasma. Being a large quantity in a tokamak, the plasma current can easily offer free energy if the current density profile is not well optimized[5]. In terms of the MHD energy principle, the current drive term is associated with the plasma volume integral of $-\frac{1}{2}\left|\mathbb{j}_{\parallel}/\mathbb{B}\right|\left(\xi_{\perp}^{*}\times\mathbb{B}\right).\delta\mathbb{B}_{\perp}$ term from Eq. (59), i.e., the primary drive is due to the equilibrium parallel current $j_{||}$. In MHD theory, the current drive often manifests in the value of safety factor q, which is roughly inversely proportional to the toroidal current integrated over a plasma volume enclosed by the given magnetic flux surface as shown in Eq. (1). Therefore, many current driven MHD instabilities are controlled by the safety factor q. Below is a list of important MHD modes that are at least partly driven by the plasma current.

The most important current driven MHD mode is the n=1 ideal EK, which becomes unstable when the edge safety factor drops below 2 in a tokamak plasma[6]. This results in the ideal external kink instability which usually leads to plasma disruption. It is difficult to overcome this stability limit but partial success has been achieved in recent experiments via active control of this instability (Hanson 2014, Piovesan 2014). A less severe, but often observed current driven instability is the IK mode, which can be unstable when the core safety factor q drops below 1. This is often manifested as the sawtooth instability in experiments. At higher values of edge q close to a low order rational number, the edge localized kink-peeling mode can be unstable. Similarly, if the safety factor profile is non-monotonic along the plasma minor radius and q_{min} (the minimum q value) is close to a low order rational number, an unstable infernal mode can occur[7]. Finally, the plasma current density profile, alone or in combination with the plasma pressure, determines the tearing-mode index Δ' (Glasser 1975) from the ideal region, which directly affects the tearing mode instability. The plasma current density profile is also directly related to the magnetic shear. A strong (positive) magnetic shear is generally stabilizing for most of MHD modes[8].

---

[4] The bootstrap current is a toroidal current driven by non-ideal effects by the temperature and density gradients. It arises from trapped particle effects.

[5] We note that large plasma current offers good energy confinement in tokamak plasmas.

[6] The edge safety factor is measured in terms of the edge q_s for a limiter plasma, and is often measured in terms of q_{95} (q at normalized $\psi = 0.95$) for a divertor plasma.

[7] More precisely, a finite pressure gradient is also required to drive the instability. The infernal mode can therefore be regarded as a MHD instability driven by both plasma current and pressure.

[8] Negative magnetic shear (which occurs in plasmas with non-monotonic q-profiles) can stabilize tearing mode.

Resistivity effects

Many ideal MHD instabilities have resistive counterparts. Typically, the most interesting situation is that the ideal branch is stable within certain parameter space, but taking into account the finite plasma resistivity qualitatively changes the picture by rendering the mode unstable, resulting in a resistive instability. Prominent examples are the tearing mode, the resistive interchange, the resistive internal kink, and the resistive external kink mode. Of course, the plasma resistivity also modifies (mostly enhances) the growth rate of an unstable ideal counterpart and the degree depends on the corresponding ideal instability[9].

Within the MHD theory, the key physics associated with the plasma resistivity is that the ideal frozen-flux constraint is not valid. The plasma displacement and the magnetic field perturbation can evolve separately[10], creating additional freedom for the plasma motion and for the perturbation to grow. This is the fundamental mechanism for the destabilization of the resistive instability when the ideal counterpart is stable.

On the other hand, there are also cases where the plasma resistivity plays a stabilizing role by dissipating free MHD energy via the resistive layer. One example is the fishbone instability, which is stabilized by finite plasma resistivity (Biglari 1986, Wu 2018). Another example is the resistive-plasma resistive-wall mode (RPRWM), where the global ideal MHD instability resistive-wall mode (RWM) couples to the tearing mode localized near a rational surface. The favorable average curvature stabilization of the tearing component within the resistive layer helps to stabilize the RPRWM (He 2014). This mechanism applies when the coupling between the ideal and the resistive components is strong.

The TM is probably the most studied resistive instability (Glasser 1975, Hegna 1994). Both linear and non-linear theories are well developed. Several approaches have been established to study resistive instabilities, including the asymptotic matching, typically employed in analytic theory but also be useful in numerical codes.

Effects of plasma toroidal flow

Equilibrium toroidal plasma flow, as well as flow shear can affect MHD instabilities[11]. The stabilization mechanism varies depending on the type of MHD mode. First, for the effect purely from the flow amplitude, imagine a flow that is uniform along the plasma minor radius. For many localized MHD modes, this uniform flow merely introduces a Doppler shift to the mode frequency (a change of reference from the laboratory frame to the rotating plasma frame), without modifying the mode growth rate. This may, however, be different for more global (in terms of plasma displacement) MHD modes. Two important examples are the RWM and the internal kink (IK) modes. The RWM does not rotate with the plasma and therefore is subject to continuum wave

[9] For instance, the plasma resistivity typically has very minor effect on an ideal external kink mode which grows at the Alfvenic time scale.

[10] As a consequence, the magnetic topology is allowed to change near a mode rational surface, resulting in magnetic islands.

[11] Plasma poloidal flow can in principle also affect MHD instabilities such as the RWM, but this is often not a significant concern, because poloidal flow is often slow in a tokamak plasma due to neoclassical damping. Parallel plasma flow (along magnetic field lines) typically does not have significant effect on the MHD instability (Xia 2019).

damping due to plasma flow. The IK is subject to a gyroscopic stabilization when the Mach number reaches a value comparable to the inverse aspect ratio.

On the other hand, flow shear typically destabilizes macroscopic MHD modes (unlike microscopic instabilities for which flow shear often plays a stabilizing role). The fundamental destabilization physics originates from the Kelvin-Helmholtz mechanism, where two adjacent fluid elements flowing at different velocities develop an unstable motion that eventually leads to turbulent flow. Flow shear destabilization has been found for many MHD modes, such as the RWM and the IK.

On the other hand, flow shear may help to stabilize certain MHD modes. One example is the observed 3/2 NTM island reduction from plasma flow in DIII-D experiments (La Haye 2009. Reduction of the tearing instability index by plasma flow shear was proposed as an explanation, and experimentally, the mode is observed to grow when the rotation is reduced (Politzer 2008, Solomon 2013). Differential flow also helps to stabilize the double tearing mode (Dewar 1993), by decoupling the two rational surfaces.

Energetic-particle effects

Energic particles (EPs), although a minority particle species in fusion plasmas in terms of particle number density, often play important roles in MHD instabilities. There are two main reasons for this. (i) EPs have much higher energy than the background particle species, so that the EP pressure, which is the product of the particle density and temperature, can sometimes contribute a significant fraction to the total plasma equilibrium pressure[12]. This modification of equilibrium pressure due to EPs changes the MHD stability behavior of pressure driven modes. (ii) EPs can also directly interact with MHD perturbations and thus modifying the instability and even triggering new instabilities.

There are two key physics mechanisms involved in the direct interaction between EPs and MHD modes. One is the wave-particle Landau resonance[13], where certain frequencies associated with the EP motion match the frequency of the MHD perturbation. Free energy transfer between EPs and the MHD mode then ensues. The direction of the energy transfer, which determines whether the MHD mode is stabilized or destabilized, depends on many factors. The other physics mechanism is associated with trapped EPs, whose bounce motion forms a banana orbit that rotates along the toroidal angle of a tokamak. This toroidal motion of the banana orbit tends to conserve the vertical flux enclosed by the center line of the banana (Northop 1963). If the toroidal rotation frequency of the banana orbit is faster than the perturbation frequency, the mode can be stabilized.

Examples of EP stabilization of MHD modes include the internal kink (Porcelli 1991, Graves 2004), the RWM (Chapman 2009, Liu 2010), and the TM and NTM (Hegna 1989, Cai 2011)[14]. Examples of EP triggering of MHD instabilities include the fishbone (Chen 1984, Coppi 1986), e-fishbone (Wong 2000), Alfven eigenmodes (Fu 1989), and energetic particle modes (Chen 1994).

---

[12] As an example, fusion born alphas contribute more than 20% to the total pressure in an ITER advanced plasma scenario (Liu 2010).

[13] MHD modes can often be treated as (stable or unstable) waves. Wave-particle Landau resonances are used in many contexts in fusion devices. An important application is plasma heating by launching radial waves with frequency matching the cyclotron frequency of thermal ions or electrons.

[14] TM/NTM stabilization by EPs may involve either direct interaction (Hegna 1989) or another, indirect way where EPs modify the external tearing index (Liu 2012).

Principal MHD instabilities

Overview

MHD instabilities are generally driven by a combination of electromagnetic and thermodynamic forces. The basic equilibrium relation Eq. (33) $\nabla P = \mathbb{j} \times \mathbb{B}$ describes the balance of these forces. Normally, instabilities are categorized as being either 'current-driven' or 'pressure-driven' depending on what is considered to be the major drive. For example, at zero pressure, the instabilities are naturally considered as 'current-driven'. Onset criteria can be obtained in this limit. With pressure, instabilities that arise when the current driven mode onset criteria are not satisfied are then usually considered as pressure-driven. This categorization works quite well in most cases since there are features in the mode structure that correspond to the distinction.

Within this categorization, a number of other labels are applied to various MHD instabilities. Early in the history of MHD, the first instabilities studied were called kink, flute, and sausage modes. The label 'kink' or 'External kink' is largely synonymous with 'current driven kink'. These are driven by a current density gradient or jump at the edge. Flute modes are an alternative term for pressure driven interchange modes. The sausage instability corresponds to pressure driven modes with poloidal mode number $m = 0$. Peeling modes are a subcategory of the external kink, corresponding to toroidal mode numbers $n > 1$.

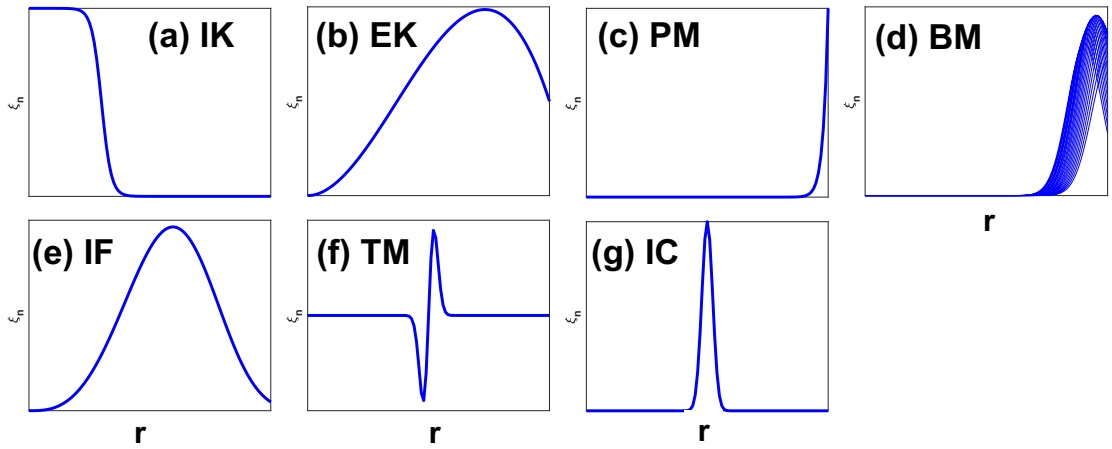

Fig. 3. Sketch of eigenmode structure, in terms of radial plasma displacement, for typical MHD instabilities: (a) internal kink (IK), (b) external kink (EK), (c) peeling mode (PM), (d) ballooning mode (BM), (e) infernal mode (IF), (f) tearing mode (TM), (g) interchange mode (IC).

Ballooning modes are pressure driven. Normally the label is applied to the high-n version but pressure driven modes at intermediate and low n all have the characteristic 'ballooning structure' with a large coherent motion on the outboard side as field lines interchange locally there. Interchange modes are simply ballooning modes in the low shear limit where the interchange is global along the field line. Infernal modes, similarly refer to localized instabilities destabilized by a large pressure gradient in a locally low shear region. Bear in mind that these labels are really only valid in certain limits; most instabilities in real plasmas are a mixture of different features. The peeling-ballooning modes understood to be responsible for ELMs are a prime example of instabilities that defy characterization as either current driven or pressure driven (Snyder 2002). Both the pressure and current-density gradients are important drivers. The internal kink,

responsible for the sawtooth phenomenon in tokamaks is another example. In a torus, the ideal internal kink is stable at zero pressure (Bussac 1975), but has a very low β limit. The β limit also vanishes if the wall is removed (Turnbull 1989).

Axisymmetric modes are the ideal $n = 0$ instabilities. These are essentially current-driven in the sense that they are largely independent of the pressure and depend only on the gross features of the current profile. For a circular cross section, this mode is stable. In an elongated tokamak, the mode is a vertical shift ($m = \pm 1$).

For non-ideal modes, resistivity is an important driver of instabilities. Resistivity allows rational closed field lines to break and reconnect with a different topology. Two different modes can form corresponding to two different parities. An external kink can result when two adjacent flux surfaces interchange position by breaking and reconnecting. This is the resistive version of the ideal kink mode. Alternatively, the closed rational surface can split with the two parts moving apart and opening up a magnetic island. The tearing apart of the surface provides the name 'tearing mode'. This mode has no counterpart in ideal MHD. Figure 3 shows how various MHD instabilities qualitatively look like, in terms of the radial distortion of the plasma caused by the instabilities.

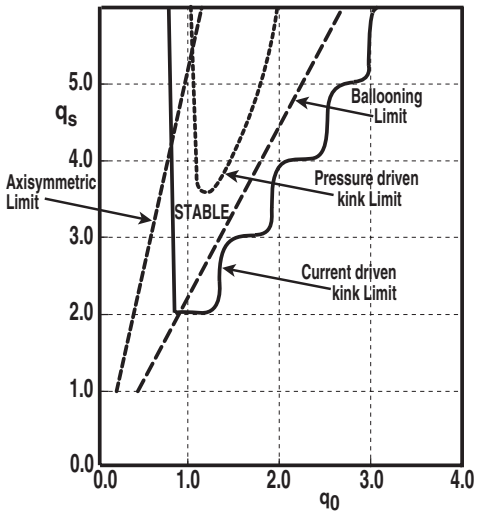

Fig. 4. Regions in parameter space of different modes in the q_0 , q_s parameter space. Here, q_0 and q_s are the safety factor on axis and at the edge.

Wesson identified the regions unstable to current driven modes in a model cylindrical plasma in the space of q_0 and q_s/q_0 (Wesson 1978). Here, q_0 and q_s are the safety factor on axis and at the edge. These are the most important parameters determining current-driven instabilities. Figure 4 is a corresponding 'Wesson diagram' replotted in terms of q_0 and q_s for a generic strong Dee shape in toroidal geometry with a monotonic current density profile and zero β. The boundary follows a generic stair-step pattern with steps at or near rational values of either q_0 or q_s. Changes in the current profile shape for fixed q_0 and q_s change the steepness of the staircase. Pressure tends to smear the boundaries. However, there is no stable range in particular for $q_s < 2$ for any current profile. Superimposed is the axisymmetric stability boundary and the general form of the stability limit against pressure driven kink modes for a fixed, finite β_p. The stable region is in the center. The slope of the axisymmetric boundary varies with ℓ_i. With increasing β_p, the pressure driven

kink boundary dips to lower q_s. A generic ballooning stability boundary is also shown; again, the slope in this diagram varies with ℓ_i, also with β_p.

Axisymmetric modes

The axisymmetric instability is a vertical displacement of the plasma cross section in a vertical magnetic field. The plasma consists of a toroidal current in a vertical magnetic field. One can imagine a rigid elliptical cross section like an egg being squeezed by the vertical field. The shape of the egg diverts the lateral squeezing forces into a net vertical force and the egg slips rigidly in the field. Stability is determined then by the shape of the egg relative to the vertical field. With an elliptical cross section, the egg slips easily. Image currents in the wall generated by Lenz's Law, however, provide a stabilizing reaction force by opposing the fields generated by the vertical motion.

For a circular cross section plasma, the current loop is stable to a vertical shift. Essentially, for the plasma to slip up or down from its equilibrium position, it has to compress the external vertical field, requiring a source of energy. However, an elongated elliptical plasma can slip vertically with less distortion of the vertical field. For some elongation, the plasma becomes unstable to this motion and disrupts. For a large aspect ratio ellipse, the eigenmode is the pure axisymmetric vertical shift characterized by toroidal mode number $n = 0$ and an equal mix of poloidal mode numbers $m = \pm 1$ with constant amplitude as a function of radius;

$$\xi(r, \theta, \phi) = \xi_0\left(e^{i\theta} + e^{-i\theta}\right) \sim \xi_0 \cos\theta. \qquad (60)$$

In a torus there is some deviation from this due to the $1/R$ dependence of the fields. Additional $m = \pm 3$ components appear in a Dee shape and a stronger radial profile dependence of the $m = 1$ shift plus higher m components appear with higher order shaping.

In actual experiments, the instability is stabilized by a nearby surrounding conducting wall in which image currents are induced to oppose the magnetic field changes, preventing the perturbed flux from penetrating the wall (Lenz's Law). With finite resistivity, the image currents decay in a characteristic L/R time and requires active feedback to fully stabilize it. The axisymmetric instability is well understood. Calculations of the ideal eigenfunctions have been shown to match the measured boundary displacements. In most cases, the observed open loop resistive wall growth rate can easily be fitted by simple plasma models assuming a rigid vertical displacement, sufficient for the feedback algorithms.

Internal kink, sawtooth, and fishbone

The IK mode, with the toroidal mode number of n=1 and the poloidal mode number of m=1,[15] is an instability predicted by ideal MHD theory in early stage of fusion research. However, some of the aspects associated with this mode, in particular the non-linear aspects and the interaction between this mode and energetic particles, are still active research areas.[16]

From the MHD viewpoint, the primary driving mechanism for the IK instability is the free energy associated with the plasma current. More precisely, a critical condition for the mode instability is that the safety factor on the magnetic axis, q_0, should be below 1. This condition is, however, not

[15] In a toroidal plasma, the n=1 internal kink mode, as a linear eigenmode, has many poloidal harmonics. The m=1 harmonic is the dominant one.

[16] For recent research on the internal kink and sawteeth, see for example (Jardin 2020).

sufficient for an unstable IK. In a tokamak plasma, the IK becomes unstable only if the plasma pressure exceeds certain critical value. The mode growth rate γ, within the MHD framework, is in fact proportional to $(1-q_0)\left(\beta_{pcr}^2-\beta_p^2\right)$, where β_{pcr} is the critical value typically below 0.4. This is the well-known Bussac criterion (Bussac 1975) for the IK instability. This criterion shows that the IK is also partly driven by the plasma pressure.

Because the mode growth rate is proportional to $(1-q_0)$ (provided that the Bussac pressure limit is exceeded), the IK instability strength depends critically on the proximity of the on-axis safety factor to unity. In typical tokamak discharges, the on-axis safety factor is not far from 1, resulting in an IK that is not far from the marginal stability. A weakly unstable IK is subject to a range of non-ideal effects beyond the ideal single-fluid MHD description. Important effects include the plasma diamagnetic stabilization[17], the plasma resistivity, the drift kinetic effects associated with plasma particles. On top of these non-ideal effects, the plasma equilibrium toroidal flow also affects the mode stability. In what follows, we briefly discuss each of these effects.

A weakly unstable IK is often subject to strong diamagnetic stabilization in a tokamak plasma. This is because the typical mode growth rate in this case is comparable to the thermal ion diamagnetic frequency. The dispersion relation for the mode (complex) frequency ω satisfies $[\omega(\omega_i^*-\omega)]^{0.5}=-\delta W$, where ω_i^* is the thermal ion diamagnetic frequency and δW is the normalized perturbed potential energy.[18] In the absence of the diamagnetic stabilization and for a purely growing IK mode, the mode growth rate scales linearly with the perturbed potential energy.

Plasma toroidal flow can be either stabilizing or destabilizing to the IK. The fundamental physics mechanism for the flow stabilization of the IK is the so-called gyroscopic stabilization (Wahlberg 2000), where the perturbation, which has a rigid structure, is stabilized by fast rotation. The required rotation speed for full stabilization of the mode has to be very large (a large fraction of sound speed). The flow shear, on the other hand, can destabilize the IK essentially due to the Kelvin-Helmholtz type of mechanism. Associated with toroidal flow are various inertial forces (centrifugal and Coriolis forces), which can be either stabilizing or destabilizing depending on the equilibrium profiles (Wu 2019).

Non-linear evolution of the IK often manifests itself as the sawtooth phenomenon, which is observed in experiments. There are different theoretical models for sawteeth. The first and probably the most well-known model is the cold bubble model (Kadomtsev 1975), where full magnetic reconnection was assumed within the q=1 surface during the non-linear evolution.

Lastly, drift kinetic effects, in particular those associated with toroidal precession of trapped energetic particles (EPs), can have significant influence on the IK stability and the sawteeth behavior.[19] These effects are well summarized by the Porcelli model (Porcelli 1991), where three different criteria were proposed to judge the IK instability and the subsequent onset of sawteeth.

---

[17] The diamagnetic stabilization of IK is often referred to as the finite Larmor radius (FLR) effect in literature, since this effect eventually originates from the FLR of thermal ions.

[18] δW here is normalized by the plasma inertia. As usual, $\delta W<0$ indicates free potential energy that drives instability.

[19] Drift kinetic effects from thermal particles can also stabilize the IK (Hu 2006), although the effect is often not dramatic.

These Porcelli criteria have been successfully applied to interpret many experimental results in tokamak plasmas.

Drift kinetic effects of EPs not only stabilize the IK, but can also drive a new type of instability called the fishbone mode (FB)[20] (Chen 1984, Porcelli 1991). The fundamental physics here is the wave-particle Landau resonance, where an otherwise stable IK absorbs free energy from EPs, and thus becomes unstable. Since the mode is driven unstable by EP, the mode frequency matches that of the characteristic frequency of the drift motion of EPs. The most common case is again the toroidal precession of trapped EPs. Another drive is associated with diamagnetic rotation of EPs. Plasma resistivity often stabilizes the FB (Biglari 1986, Wu 2018) – an effect opposite to that for the IK. For the FB, the resistive layer dissipates the free energy.

EK/Resistive-wall modes (RWMs)

There are two drive mechanisms for the external kink instability, the plasma pressure and the plasma current. The purely current driven EK mode has been studied since early on in fusion research (Shafranov 1970, Wesson 1978). A key milestone in realizing the importance of pressure effects was the discovery of the Troyon β limit (Troyon 1984), showing that the maximal achievable normalized plasma pressure, before the discharge disrupts, scales in proportion to the normalized plasma current, as shown in Eq. (41).

Plasma pressure is the most typical drive in present and future tokamak devices. This mechanism resembles the ballooning drive. In fact, the eigenmode associated with the pressure driven EK is typically localized at the outboard low-field side of the torus, similar to ballooning instability. This type of EK is therefore also often called kink-ballooning instability. An important distinction with the ballooning instability, however, is the toroidal mode number associated with the perturbation. The EK is the long wavelength global MHD instability along toroidal (and poloidal as well) angle, with the typical toroidal mode number of $n = 1 - 3$, while the ballooning instability has typical toroidal mode numbers greater than 10.

For the EK driven unstable in a low-pressure plasma by the plasma current, when the nq_s value (in a limiter plasma) is just below an integer m, an instability results with toroidal mode number n, and predominantly poloidal mode number m, which causes a large plasma displacement near the plasma edge. For $n > 1$ and $m > 2$, this instability is often called a kink-peeling mode. When the plasma current is sufficiently high in a limiter plasma that q_s is below 2 (Wesson 1978), this always triggers a strongly unstable $n = 1$ EK which leads to plasma disruption if not suppressed.

In a plasma with a divertor configuration, the edge safety factor is large (mathematically infinite at the separatrix). The associated large magnetic shear near the plasma edge can stabilize the resulting mode (Webster 2009). Despite the magnetic shear stabilization, a disruptive instability is still often observed in divertor experiments, when the safety factor at the 95% flux surface, q_{95}, approaches 2.0. This puzzle was recently resolved by invoking the effect from a steep edge plasma resistivity profile (Turnbull 2016).

Independent of the drive mechanism, it has been found that the presence of an ideal conducting wall, located sufficiently close to the plasma, can stabilize the ideal EK instability up to a certain limit. In reality, the wall almost always has finite conductivity. This allows partial escape of the

[20] The word "fishbone" originates from the characteristic magnetic signals observed in experiments, which is actually a result of non-linear interaction between the instability and EPs.

perturbed radial magnetic field, at a time scale comparable to the eddy current decay time in the resistive wall. As a result, the EK again becomes unstable in the q_s or q_{95} parameter windows as described above, but now on a much longer time scale. This slowly growing instability is called the RWM (Chu 2010). Note that the resistivity here refers to that of the resistivity wall, not the plasma.[21]

The eigenmode structure of the RWM still remains global, similar to that the EK.[22] The mode growth rate is, however, significantly reduced as mentioned. This has several significant implications. (i) The presence of this residual instability means that the RWM can potentially still cause a serious disruption of the plasma. (ii) The much lower growth rate, or in general much lower (complex) mode frequency, implies other physics beyond ideal MHD may play important roles. (iii) The much longer time scale of the RWM growth, in milliseconds or longer, also makes it practical to design an active control system to actively stabilize the mode.

There exist several passive stabilization mechanisms for the RWM utilizing additional physics beyond ideal MHD. The first important effect is continuum resonance damping of the mode in a toroidally rotating plasma. Unlike many other MHD modes, the RWM, even in the linear regime, does not rotate with the plasma. A tokamak plasma typically rotates at a frequency of several percent of the Alfven frequency along the toroidal direction.[23] The RWM, on the other hand, has a frequency that is of the same order of the much smaller inverse wall time; the RWM appears to be essentially "locked" to the resistive wall. The mode thus rotates in the plasma frame, opening the possibility of Landau resonances between the mode and various continuous waves (which rotate together with the plasma) in the plasma, such as the shear Alfven waves and sound waves (more precisely slow magneto-acoustic waves). Since these continuum waves are stable, they can tap free energy from the RWM through resonances, thus stabilizing the mode. Such a mechanism was discovered numerically in a seminal work by Bondeson (Bondeson 1994) and later analytically confirmed (Betti 1995).

Numerical modeling finds that the above stabilization mechanism often requires a plasma toroidal rotation of several percent of Alfven frequency (Bondeson 1994, Chu 1995, La Haye 2004), in order to fully suppress the RWM in a tokamak plasma. Later experiments (Reimerdes 2007), where the plasma toroidal flow was intentionally kept slow by balanced neutral-beam injection, the RWM instability did not occur even when the plasma pressure exceeded the no-wall Troyon limit, contradicting theory predictions. The puzzle is resolved by evoking additional physics, namely drift kinetic theory (Hu 2004), where Landau resonances between the mode and the drift motion of plasma thermal particle species become important. Indeed, because the toroidal precessional drift frequency of trapped thermal particles (both ions and electrons) is typically very low (well below the thermal particle diamagnetic drift frequency), a strong resonance occurs if the RWM also happen to have small frequency in the plasma frame, which is the case when the plasma toroidal rotation is slow. Since then, precessional drift-kinetic stabilization of the RWM has been

---

[21] The resistive-plasma resistive-wall mode is another interesting topic that has been under extensive studies in recent years (Betti 1998, Finn 2006).

[22] Subtle differences in the mode structure for the resonant harmonics near the mode rational surfaces appear for the RWM in a toroidal plasma, which often do not play a significant role.

[23] There are many reasons for finite toroidal rotation, e.g., due to toroidal momentum source associated with tangential neutral-beam injection, the presence of intrinsic toroidal torque.

confirmed by extensive numerical modeling work (Liu 2008, Chapman 2009, Berkery 2010). The MHD-kinetic hybrid description of the RWM instability still remains an active research area.

Resistive interchange/TM/NTM/locked modes

The resistive interchange (RI) mode and the TM are the two most important spatially localized resistive instabilities. There are many interchange instabilities in fusion plasmas[24], but those with finite toroidal mode number and poloidal mode number $m > 1$ are most important Compared to the TM, the interchange mode has opposite parity. More specifically, if we define the mode parity by the associated radial plasma displacement[25], the interchange mode has even parity (*i.e.*, symmetric about the mode rational surface) and the TM has odd parity (*i.e.*, anti-symmetric about the mode rational surface).

Both instabilities are driven by finite plasma resistivity (assuming that the ideal counterparts are stable), by allowing a change in the magnetic topology near the rational surface. According to the Mercier criterion (Mercier 1960), the ideal interchange is unstable if a quantity $D_I = D_R + \frac{1}{2}$ is positive. D_R is proportional to the equilibrium pressure gradient at the mode rational surface. However, the resistive interchange is unstable if D_R is positive. An equilibrium with zero or negative D_R, on the other hand, can be unstable to the TM. Since the latter typically holds for a tokamak plasma, the RI mode is usually not as critical as the TM[26]. The following will therefore focus on the TM and its neoclassical counterpart, the NTM.

The linear TM instability is often driven unstable by the plasma current profile. Because the mode displacement is strongly localized near a rational surface, the instability is often studied via a matching procedure, where the ideal MHD equations at marginal stability[27] are solved and the solution is matched to that of the resistive MHD equations within a narrow layer around the rational surface. Typically, the perturbed radial field (or magnetic flux) is used to perform the matching procedure. The logarithmic derivative of the outer ideal solution experiences a jump across the mode rational surface. This jump, denoted as Δ', characterizes the free energy associated with the equilibrium current density gradient that drives the TM unstable. The outer solutions are matched to the non-ideal solution obtained in a narrow inner layer around the rational surface to produce a continuous solution. In a pressure-less plasma, the matching condition yields a simple relation between the mode growth rate γ and Δ',: $A\gamma^{5/4}\eta^{-3/4} = \Delta'$, with η being the plasma resistivity and $A > 0$ a geometric factor. This dispersion relation implies that the TM is unstable whenever the tearing index Δ' is positive, and that the mode growth rate scales as $\gamma \sim \eta^{3/5}$.

In an equilibrium with finite pressure (more precisely with finite negative D_R), an important, so-called favorable average curvature, effect becomes important and modifies the TM dispersion relation to a form $A\gamma^{5/4}\eta^{-3/4}\left(1 - BD_R\gamma^{-3/2}\eta^{1/2}\right) = \Delta'$, where $B > 0$ is now another geometric factor (Glasser 1975). This new physical effect, coming from the resistive layer solution, qualitatively changes the TM stability criterion. Then, Δ' has to be larger than a critical positive

---

[24] For instance, the so-called sausage instability in a Z-pinch can also be viewed as an interchange instability based on the fundamental drive mechanism.

[25] The parity of the perturbed radial field is opposite to that of the radial displacement due to the ideal MHD constraint.

[26] Even if a resistive interchange is unstable in a tokamak plasma, it can be easily stabilized by plasma rotation.

[27] This assumption is valid for the TM, because the mode frequency is several orders of magnitude smaller than the Alfven frequency. The latter is characteristic for the ideal region solution.

number, in order to ensure the TM instability. In other words, this average curvature effect plays a stabilizing role (thus "favorable") to the TM instability. This is one of the key physics associated with the TM in a toroidal plasma[28].

Because of the strong radial localization of the instability, non-linear effects are important for the TM. A critical consequence of a developing TM instability is the change of the magnetic topology near the mode rational surface, where a chain of magnetic islands with helical structure forms. Essentially all the non-linear effects are related to the local change of the plasma current in the presence of magnetic islands. The first non-linear effect was identified by Furth et al. (Furth 1963), leading to an algebraically (instead of exponentially) growing magnetic island. Later studies identified an important role played by the neoclassical effect associated with the bootstrap current (Qu 1985, Fitzpatrick 1995, Wilson 1996), that modifies the TM stability and results in the neoclassical tearing mode (NTM). The bootstrap current is stabilizing to the TM. If, however, a portion of the bootstrap current is missing in the presence of $3D$ magnetic islands[29], the stabilizing role is reduced and the NTM can be triggered. Note that all these effects involve the finite island size and are thus intrinsically non-linear, requiring a threshold in the island size[30].

The time evolution of the NTM islands is well described by the quasi-linear Modified Rutherford Equation (MRE), which includes these effects, but excludes nonlinear coupling to other toroidal mode components with different n. The other non-linear effect is the interplay between a growing island and the plasma toroidal rotation. This is important for a full understanding of locked modes (LMs), which correspond to the locking of an NTM to the wall. This is, in fact one of the major causes of plasma disruptions in experiments (besides VDE and EK discussed before). Mode locking, as well as NTM control, will be presented in a later section on MHD stability control.

Toroidal Alfven eigenmodes[31]

The Hermitian nature of ideal MHD implies that the squared frequency, ω^2, which is the eigenvalue, is always real. Stable modes correspond to those with non-negative ω^2. In the cylindrical approximation, it can be shown that the ideal MHD spectrum consists of a possible set of discrete or isolated unstable modes and a continuum of irregular modes on the stable side arising where the coefficient of the second order term in the eigenvalue equation vanishes. These continuum modes are highly localized at the point where the coefficient vanishes and actually consist of two overlapping continua corresponding to sound waves and Alfven waves, respectively. In the ideal limit, they have infinite energy but are regularized by non-ideal effects. On the unstable side, the eigenmodes correspond to the array of physical ideal MHD instabilities discussed above. There can be a finite (or zero) number of unstable modes or a countably infinite number. In the latter case, generally corresponding to violation of the local Mercier criterion, the

---

[28] Later studies found additional interesting layer physics that modify the TM dispersion relation, e.g., the large island correction that restores the $\gamma \sim \eta^{3/5}$ scaling at high resistivity value (Militello 2004), the cancellation effect (to the favorable curvature stabilization) due to anisotropic thermal transport (Lutjens 2001, Connor 2015).

[29] There can be different ways to change the bootstrap current, e.g., due to particle flattening of the plasma pressure profile inside the magnetic islands (Fitzpatrick 1995) or due to induced polarization current (Wilson 1996).

[30] There have been discussions on triggerless/seedless NTM which likely originates from a linearly unstable TM due to large and positive Δ'.

[31] See Chapter 12.08 of this encyclopedia by Gorelenkov and Sharapov for a detailed discussion on EP-driven MHD instabilities.

eigenvalues have an accumulation point at marginal stability. The stable spectrum is shown in Fig. 5. In ideal MHD the stable continuum modes of course are purely oscillatory and have no damping or drive, lying on the imaginary axis in ω space. In reality, they tend to be strongly damped by various non-ideal effects, most notably ion Landau damping.

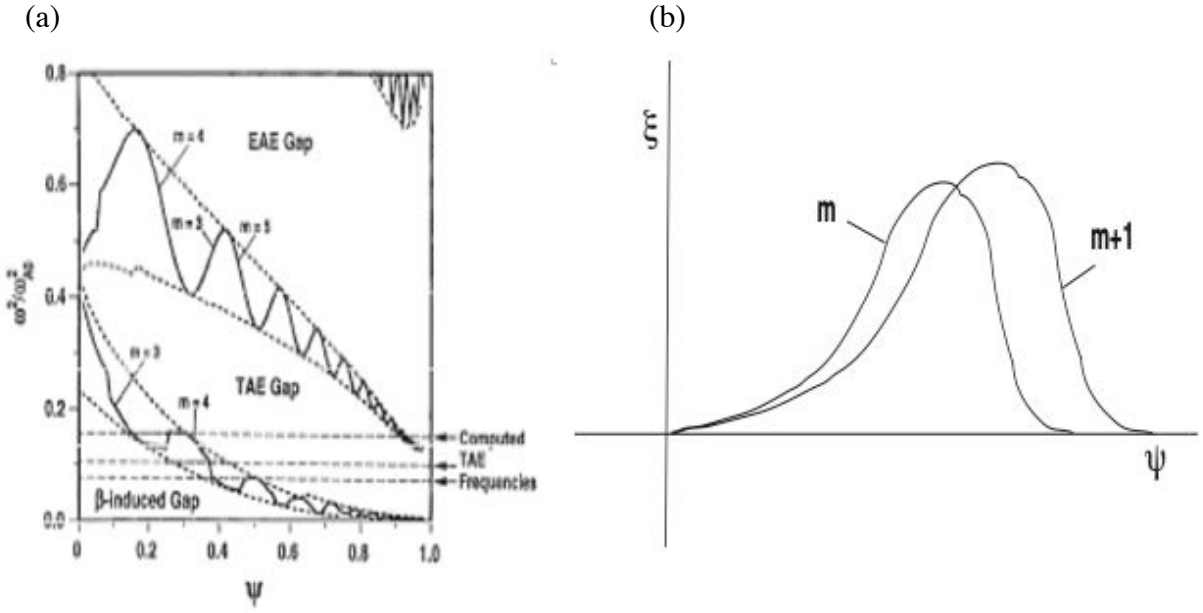

Fig. 5. (a) The continuous spectrum formed from frequencies ω^2, at which the coefficient vanishes against radius for different m and showing the TAE BAE and EAE gaps. (b) TAE mode structure consisting of coupled m and $m+1$ components.

This situation persists in toroidal geometry but with an important modification. In the cylinder, there is a separate continuum for each poloidal mode number m. In the torus, the equations for different m are coupled and near the crossing points, degenerate perturbation theory applies and the curve crossings are replaced by the reconnected curves shown, leaving gaps in the frequency. This is shown in Fig. 5(a). Within the gaps, global regular eigenmodes appear in the Alfven continuum at isolated frequencies. These consist of coupled m and $m+1$ components with a typical example shown in Fig. 5(b). Again, in ideal MHD these are purely oscillatory modes with no damping. However, the non-ideal damping of the irregular continuum modes is inversely proportional to the radial wavelength and is greatly weakened for this global mode. In particular, when the gaps overlap across a wide radius, there is no radius at which this global mode interacts with or couples to a localized continuum mode and the damping becomes small. Instead, these modes are relatively easily driven unstable. These are known as the toroidal Alfven modes (TAEs).

The frequencies of typical TAE and other similar higher frequency global modes are generally sufficiently high that the damping rates are much smaller; $\omega_{TAE} \gg \gamma_{damp} \sim \gamma_{drive}$. In that case, the ideal estimate of the real frequency is generally sufficiently accurate and the drive and damping can be computed using the computed ideal mode. The non-ideal effects simply add an additional imaginary part to $\omega_{TAE} \rightarrow \omega_{TAE} + i(\gamma_{drive} - \gamma_{damp})$, corresponding to a growth or damping rate. For most situations this is a valid assumption. In addition to the weakened ion Landau damping, several other non-ideal mechanisms dampen the TAE and other stable global modes. The most important of these is the so-called 'continuum damping', which results when an open gap does not

extend all the way across the radius. In that case, the TAE at one broad location couples directly to a continuum mode (irregular in ideal MHD), inheriting its large inherent ion Landau damping. Several kinetic effects provide additional damping sources but more important, result in a second global mode in the gap at higher frequency. This is known as the Kinetic Toroidal Alfven Eigenmode (KTAE) and has no MHD counterpart. The instability drive of most interest is from fast non-thermal ions via an inverse ion Landau process. Such ions are typically present in current experiments as a result of external ion heating of the plasma by either neutral-beam injection or RF waves. In future experiments, the concern is that energetic alpha particles from the fusion reaction would provide the drive.

In the case of RF waves, the waves themselves can be designed to resonate at Alfven-like frequencies and used to probe the plasma. When the external RF wave resonates with a stable MHD plasma wave as the frequency is varied, the width of the resonance peak provides a measure of the inverse of the damping rate of the mode. This technique, called MHD Spectroscopy, has been used to study the stable Alfven continuum spectrum as well as low frequency marginally stabilized MHD kink modes.

In addition to toroidicity, other geometric effects can couple the poloidal harmonics and break open new gaps in the continuum. The most important of these are ellipticity and triangularity, with their corresponding global Ellipticity Alfven Eigenmode (EAE) and Triangularity Alfven Eigenmode. With finite β, the Alfven continuum lifts off the marginal point $\omega^2 = 0$ leaving another gap below with width proportional to β_P. The gap is filled with sound wave continua. With respect to the discrete frequencies of these modes and their gaps, the effect of finite β appears to raise them by an amount roughly proportional to β_P. However, relative to the gap, the global mode moves slightly down in frequency with increasing β_p (Turnbull 1993).

This lower gap is known as the Beta-induced Alfven Eigenmode (BAE) gap (Turnbull 1993). Early experiments searching for the TAE mode also found global Alfven-like modes within the BAE gap. Numerical searching subsequently found global largely single harmonic modes sitting in this gap. Theory is somewhat complicated for these modes since the usual assumptions of small coupling to the sound waves are not really valid (the numerical calculations included it). The key physics in this mode is compressibility. The gap and mode are associated with the energy required by a global Alfven wave to compress as it moves in the curved torus. This is in contrast to a sound wave that propagates as an actual compressional wave. Ignoring compressibility to eliminate the sound waves also eliminates the BAE physics.

Several other Alfven eigenmodes were discovered in experiments that revealed so-called 'chirping modes', in which the observed frequency 'chirped up' until the mode disappeared or would be converted to a TAE mode. Ideal stable modes associated with these were subsequently found in continuum gaps that resulted from these particular discharges having an off-axis reversal in the q profile. Hence, they were called Reverse-shear Alfven Eigenmodes (RSAEs) (Kramer 2006). The gap was determined at any time by q_{min} which varied in time and explained the chirping behavior. Intermittent behavior sometimes results from a periodic expulsion of the fast ions driving the mode unstable, thereby suddenly stabilizing it, and a reforming of the previous beam distribution and plasma conditions.

Edge localized modes (ELMs)

Edge localized modes (ELMs) are instabilities driven by the large edge pedestal pressure gradient and its associated bootstrap current in tokamak H-mode plasmas. ELMs are generally divided into different types such as Type I-IV and "grassy" (Leonard 2014). Not all these types of ELMs are driven by macroscopic MHD modes[32]. The focus in the following discussion is on Type-I ELMs which have macroscopic MHD origin. More importantly, Type-I ELMs have been experimentally demonstrated to lead to unacceptable material erosion in future reactor-scale tokamaks by inducing thermal and particle fluxes onto the plasma facing components.

Type-I ELMs can be explained by a model for edge localized modes as predominantly ideal instabilities with low to intermediate toroidal mode number. This idea was around for some years (Turnbull 1986, Strait 1994b), and was proposed in later years on the basis of ideal MHD stability calculations for DIII-D discharges using a model for the pressure driven bootstrap current included in the equilibrium reconstruction and DIII-D ELM experiments (Zohm 1995, Ferron 2000, Lao 2001, Snyder 2002). This current produces a large current density peak near the edge of the plasma sufficient to destabilize low to intermediate n instabilities driven partly by that current density gradient (peeling mode component) and partly by the edge pressure gradient (ballooning mode component). The peeling-ballooning model has since been incorporated into a model known as the EPED model that combines the MHD peeling-ballooning stability limit with other non-MHD limits to predict the actual ELM onset (Snyder 2009, Snyder 2011). This was made possible by the development of the ELITE (Edge Localized Instabilities in Tokamak Experiments) edge stability code to efficiently compute intermediate to high n modes (Wilson 2002, Snyder 2002).

The basic MHD instabilities behind Type I ELMs are known as peeling-ballooning modes. The external kink mode, when becoming unstable at relatively high edge safety factor (more precisely at high nq_{95}), tends to localize near the plasma edge with a large kink component driven by the strong bootstrap current gradient, as well as a peeling component at the separatrix, and a low to intermediate n toroidal mode number. This is called kink-peeling mode or simply peeling mode. The other component of the Type I ELM is the ballooning mode, which is typically a short wavelength perturbation along both toroidal and poloidal angle, and is geometrically localized near the plasma outboard edge at the low field side[33]. The ballooning instability is driven by the plasma pressure, more precisely the large pressure gradient near the plasma edge. Since large pressure gradient often occurs in a H-mode plasma with large edge pedestal, the latter is the primary free energy source driving ballooning instability in a tokamak plasma.[34] Because the ballooning mode is a high-n perturbation, the full MHD equations can be significantly reduced in order to efficiently but approximately describe this instability, by dropping higher order terms in $1/n$. A critical analytic development is discovery of the so-called ballooning representation (Connor1978), which allows a more natural (in physics sense) representation of the eigenmode structure and substantially facilitates theoretical (and often numerical as well) analysis of this mode. The

[32] For instance, type-III ELM is believed to be driven by micro-tearing mode (Snipes 1998).

[33] The ballooning mode is described as local instability here in a relative sense. Sometimes, the mode with finite (but large n) is referred to as non-local, in comparison to the infinite-n ballooning mode which is localized on magnetic flux surfaces.

[34] With further increase of the plasma pressure, the ballooning mode can enter into a second stability regime (Greene 1981). This is primarily because higher pressure increases the Shafranov shift and compresses the equilibrium magnetic field lines in the low field side of a tokamak plasma, which is stabilizing for MHD instabilities.

extension of the ballooning formalism to higher order in $1/n$ enabled development of the ELITE code (Wilson 2002, Snyder 2002).

The ballooning mode is also subject to many physics effects beyond the single-fluid ideal MHD description (Connor 1988). The most important one among these effects is the diamagnetic stabilization of the mode (Rogers 1999, Hastie 2000, Snyder 2011). Based on understanding of both the ideal and non-ideal physics, a theoretical model - the EPED model (Snyder 2009, Snyder 2011) - has been developed to predict the plasma pedestal conditions for onset of Type I ELMs. The key idea of the model is the realization that the pedestal structure – both the height and width – can be constrained by two modes in a tokamak H-mode plasma. One is the peeling-ballooning constraint and the other constraint is due to a more localized, transport type of instability such as the kinetic ballooning mode. These two modes constrain the pedestal height and width following two different scaling curves, and their intersection indicates what is realizable in experiments. The EPED model has been successfully applied to a range of tokamak experiments (Snyder 2011). In addition, the model predicted the existence of, and the access route to, a new high performance plasma regime called super-H mode that was subsequently realized in experiments (Solomon 2014, Snyder 2015, Solomon 2016, Hughes 2018, Snyder 2019, Knolker 2020).

The EPED model reproduces the triggering mechanism of type I ELMs well (Snyder 2011). However, the ELMs observed experimentally represent a highly non-linear stage of the instability. For instance, the filamentary structure that is observed in experiments inside the plasma separatrix is no longer a linear ballooning instability. This is an ongoing area of theoretical research.

Finally, there are ELM-stable regimes in tokamak plasmas. These ELM-stable regimes are favorable for tokamak operations due to their benign feature and thus minimizing bursts of heat and particle fluxes reaching the plasma facing components. The L-mode is ELM-stable but is not particularly attractive in terms of energy confinement. Staying within high confinement regime, the QH-mode (Burrell 2001, Burrell 2016) and I-mode (Whyte 2010) regimes are two promising candidates without ELMs. The former often has a saturated MHD instability (the so-called Edge Harmonic Oscillation EHO) that helps to provide necessary transport in the pedestal region to avoid ELMs[35]. The latter does not require an edge pedestal in the plasma density, only pedestal in plasma temperature, which helps avoid ELM triggering but meanwhile maintains good particle and energy confinement. Furthermore, application of 3D magnetic perturbations near the plasma edge also helps to suppress ELMs and produces ELM-stable regimes (Evans 2004). Of particular recent interest is plasma with negative triangularity shape (Medvedev 2015, Ren 2016, Austin 2019, Kikuchi 2019), which can also provide an ELM-stable high confinement regime. Negative triangularity equilibria generally do not have favorable average magnetic curvature, resulting in strong ballooning instabilities that suppress the formation of an edge pedestal and hence in many cases the discharges remain in L-mode, with no ELMs, even at high power.

Stable plasma response to external 3D fields

Since plasmas consist of unbound free charges, the charges individually respond and the plasma collectively responds to applied external fields. The predominant immediate response is electromagnetic and the MHD formalism captures this well. In essence, the plasma responds by

[35] Recent studies also identified a QH-regime with wide pedestal and peculiar plasma edge flow condition, where no EHOs are needed to provide transport (Burrel 2016).

setting up Alfven waves that propagate through the system and re-establish local force balance everywhere forming a new $3D$ equilibrium state:

$$\nabla \cdot (\mathbb{P} + \delta\mathbb{P}) = \mu_0\big(\nabla \times (\mathbb{B} + \delta\mathbb{B})\big) \times (\mathbb{B} + \delta\mathbb{B}). \qquad (61)$$

This state generally has different transport properties from the original unperturbed state. For example, topological changes, particularly the presence of open field lines, can modify transport dramatically. Hence, following the MHD response, there is a longer term, transport response.

The response of the plasma is important for understanding several related phenomena. Early in tokamak fusion research, the phenomenon of locked modes plagued progress. Depending on the density, a rotating tearing mode would arise and as it grew, slow the plasma, amplifying the growth further, until the plasma locked to an error field fixed with respect to the vessel wall and usually subsequently disrupted. In studying resistive wall modes, near the stability limit it was observed that non-axisymmetric error fields were strongly amplified (Wang 2015). Third, in experiments designed to suppress ELMs, suppression was found but not by the mechanism expected. The mechanism involves the plasma response but is still not fully explained. One robust indicator of ELM controllability appears to be the edge-peeling response of the plasma to the applied 3D fields (Liu 2016), valid for both mitigation (Liu 2011, Ryan 2015, Li 2016) and suppression (Paz-Soldan 2015, Yang 2016).

When an external field is applied, the most obvious response on a particle level is that, just as in any conductor, currents flow in the plasma to oppose the changes by excluding the field from penetrating the plasma. Thus, the first response is for skin currents to flow in the edge. These currents are singular on closed rational field lines that resonate with a harmonic of the perturbed normal field: when $q = m/n$, for a field harmonic $\delta B_{n,m}(r)e^{i(m\theta - nq\varphi)}$, with a delta function radial dependence of the current density. However, finite resistivity in the plasma implies these currents decay and, unless regenerated, the field slowly penetrates. Effective regeneration of the currents can occur from plasma rotation. In pioneering work, Fitzpatrick and coworkers (Fitzpatrick 1991, Fitzpatrick 1993, Fitzpatrick 1995) demonstrated that non MHD effects result in a complex nonlinear interaction between the rotation and the perturbing $3D$ field where the field slowly removes and dissipates rotational energy as it penetrates, slowing the rotation further, and enhancing the penetration. The result is a bifurcation in the rotation, with two dynamically stable states, one at high rotation with little penetration and the other at low rotation, essentially locked in the laboratory frame, with a fully penetrated field. In between is an inaccessible dynamically unstable state. The net result of this is that by applying an external $3D$ field, the plasma subsequently slows rotation and locks to the wall. The plasma response at first expels the external field but subsequently incorporates it but in a locked stationary state. The response is a nonlinear dynamic response with suppression occurring first followed by a slow penetration depending on the resistivity and the plasma rotation.

The second major component of the plasma response is generally an amplification. This was first noted in numerical calculations of the linear MHD response where the expected suppression of specific field harmonics of the normal field component was observed at the respective rational surfaces but became finite again inside. This was attributed to coupling of the poloidal harmonics: non-resonant harmonics penetrate beyond the rational surface and drive the suppressed component back up, amplifying it.

These two parts of the MHD response are, in fact, inseparable. The total linearized response can be expressed as an expansion in the eigenfunctions of the linear eigenmodes of the ideal MHD operator $\partial^2\xi/\partial t^2 - \mathcal{L}\xi = 0$, so that $\xi = \sum_{k=1}^{\infty} a_k\, \xi_k$, where $\mathcal{L}\xi_k = \lambda_k\xi_k = -\omega_k^2\xi_k$, with λ_k being the eigenvalue and ω_k the frequency. The eigenmodes ξ_k inherently include the suppression of the resonant field harmonics at the rational surfaces and amplification in their structure. For ideal MHD, the eigenmodes of $\mathcal{L}$ form a complete orthonormal basis so any possible ideal response can be expressed completely in the expansion. The non-ideal response, however, can have contributions not in the basis corresponding to tearing solutions.

By applying an external RF field with different frequencies, the ideal MHD eigenmodes can be probed by measuring the response. For this case, by substituting the expansion for the response ξ in terms of the ξ_k into the dynamic equation of motion for a driven perturbation, $\partial^2\xi/\partial t^2 - \mathcal{L}\xi = A_0 e^{i\omega_0 t}$, one finds

$$\xi(r,t) = \sum_{k=1}^{\infty}[a_k/(\omega_k^2 - \omega_0^2)]\xi_k(r), \tag{62a}$$

$$a_k \equiv \int \xi(r,t)\, A_0 e^{i\omega_0 t} d^3r. \tag{62b}$$

The response has a resonant denominator proportional to $\omega_k^2 - \omega_0^2$ that vanishes whenever the driving frequency ω_0 coincides with a characteristic frequency of the ideal system. By measuring an aspect of the response as the frequency is varied, a series of peaks appears at these eigenfrequencies. It can also be shown that the width in frequency of the peaks is inversely proportional to the (non-ideal) damping rate. This procedure, dubbed 'MHD spectroscopy' (Reimerdes 2004) has been used in experiments to probe both the stable Alfven spectrum, identifying TAE and other Alfven eigenmodes, as well as marginally stabilized kink modes. The technique seems likely to become more prominent in the future.

The transport response follows from the changes in topology, edge conditions, and profiles due to the initial MHD response. With no topological changes, the local transport coefficients can be different as a result of changes in local profiles. When islands form, the transport is completely changed, not only from the island itself, but also because island formation necessitates formation of an associated local chaotic region. In the chaotic regions, parallel transport becomes important and competitive with perpendicular transport. Finally, when the field lines open and leave the plasma region, the global transport becomes a complex mixture of parallel and perpendicular transport, with various chaotic structures playing important roles.

There are several characteristic transport effects that are typically observed. Foremost of these is the observed rotation drag discussed above. The rotation screens the applied fields from penetrating the plasma, essentially by regenerating the screening currents formed at rational surfaces. However, the fields themselves provide a back effect by slowing the rotation. As the rotation slows, the fields are able to penetrate more easily and finally the rotation collapses to a new bifurcated locked state with fully penetrated field and decayed singular currents. The second most important observed effect is the 'pump-out' effect. The root cause of this is the formation of open field lines connecting the edge plasma layers to the exterior vacuum and material structures. Along with this pump-out effect is a generally observed reduction in core impurities.

Numerical tools

Many numerical tools have been developed for modeling MHD instabilities in fusion devices, and these tools can be classified in many different ways. We will pursue two ways of classifications

here for a list of well-known MHD codes, one is based on whether the code solves linear or non-linear MHD equations, and the other is based on which physics are included into the codes. We emphasize that what we provide below is not a full list of MHD codes that have been developed and used by the MHD community.

Many codes have been developed during the last forty years, that are capable of solving linear MHD equations in full toroidal geometry, and are well validated against experiments. Linear stability problem can always be solved as an eigenvalue problem. These codes are therefore mostly written as eigenvalue solvers, including PEST (Grimm 1976), ERATO (Gruber 1981), GATO (Bernard 1981), NOVA (Cheng 1987), MARS (Bondeson 1992), DCON (Glasser 1997), KINX (Degtyarev 1997), MISHKA (Mikhailovskii 1997), MARG2D (Tokuda 1999), MARS-F (Liu 2000a), ELITE (Wilson 2002, Snyder 2007), AEGIS (Zheng 2006), MINERVA (Aiba 2009). Some of the codes were also developed into new versions with significant inclusion of drift kinetic effects, such as NOVA-K (Cheng 1992), MARS-K (Liu 2008), AEGIS-K (Zheng 2010). The non-linear MHD codes include NIMROD (Glasser 1999, Sovinec 2004), M3D (Park 1999), M3D-C1 (Ferraro 2009), JOREK (Huysmans 2007, Pamela 2020), BOUT (Xu 1998), BOUT++ (Dudson 2009). There are also codes that solve quasi-linear MHD equations such as MARS-Q (Liu 2013).

In terms of physics, several early codes solve ideal, single-fluid MHD equations, such as ERATO, GATO, NOVA, DCON. These are all linear codes. Because associated with ideal MHD is the energy principle which has the important Hermitian property, most of these ideal MHD codes were developed based on the ideal MHD energy principle (the energy approach)[36]. There are also linear MHD codes that solve resistive MHD equations. These are typically based on the normal mode eigenvalue approach, such as the MARS code. Codes that solve extended MHD equations (including two-fluid) are often non-linear codes, such as M3D-C1, NIMROD, JOREK, BOUT++, etc. Codes that solve hybrid MHD-kinetic equations include NOVA-K, M3D-K, MARS-K, AEGIS-K, NIMROD (a version with kinetic treatment of energetic particles).

Principles of control for MHD instabilities

Fusion gain can be expressed from the fusion power P_F and input power P_I as $Q = P_F/P_I \sim \tau_E\, \beta^*\, B^2 \sim \tau_E\, p_f \beta_T\, B^2$,where τ_E is the energy confinement time and the pressure profile peaking factor p_f is defined as $p_f^2 \equiv < p^2 > / < p >^2$, and $\beta^* \equiv p_f \beta_T$. Thus, Q can be increased by increasing β_T and keeping all other factors constant. But, from the Troyon limit equation, Eqs. (41) and (42), β_T is limited by stability. Hence, one needs to optimize $\beta_T \lesssim \beta^{crit} = k_\beta \ell_i \left(I_p/aB_T \right)$ against all the important instabilities. A useful view can be reached by then rewriting the maximum fusion gain as (Lazarus 1997)

$$Q = [(R_0^2 B_T^2] \times \left[p_f\, k_\beta \ell_i\, (S^2/\kappa)\, (H^2/q_s^2) \right]. \qquad (63)$$

Here, H is a confinement enhancement factor relative to H-mode ($1 \le H \le 2$), and q_s is the boundary q, or for a divertor plasma, q_{95}. $R_0 = (R_{max} + R_{min})/2$ is the average of the maximum and minimum of the major radius of the plasma boundary. The plasma shaping enters here directly in terms of the shaping factor $S = q_s \left(I_p/aB_T \right)$ and the elongation κ. The current profile dependence appears directly through the internal inductance parameter ℓ_i.

[36] Exception is the AEGIS code which is based on the shooting method. There is also the SPEC code based on energy principle applied to multiple ideal regions coupled by special interface conditions.

The first factor enclosed in square brackets is a technological factor and a reactor has a direct cost roughly proportional to this factor. The rest contains quantities directly related to plasma physics. All but the confinement factor H are stability related and can be increased by optimization with respect to pressure peaking, cross section shape, and safety factor. The improvement in stability against pressure driven modes from cross section shaping is embodied largely in the factor S^2/κ. Q can be increased by simply increasing this factor, thereby increasing $I_p/(aB_T)$ and hence β_T. This reflects the fact that $n > 0$ stability is improved by increasing S. However, S^2/κ is limited by axisymmetric stability.

Optimization from profiles is embodied in the factors $p_f\, k_\beta \ell_i$ and $1/q_s^2$. The pressure profile peaking factor p_f is limited by $n > 0$ stability. There is also a synergistic dependence of the β_T limit on cross section and profiles. For high S, the limiting stable k_β has an inverse dependence on p_f and the product is generally optimized by low p_f, whereas at low S, the dependence of k_β on p_f is weaker. The current profile factor ℓ_i is limited by $n = 0$ stability. Stability to current driven modes provides a limit on how low q_s can be.

Advanced Tokamak Operation

By optimizing against the second factor in the expression for Q above, essentially maximizing the β_T limit, β^{crit}, a smaller, more compact tokamak with reduced major radius R_0 and B_T can match the performance of larger, high field machines by compensating the reduction. Ultimately, this requires the stabilization of instabilities. The Advanced Tokamak (AT) concept follows this route. Most AT approaches require some level of feedback. Control of the profiles pushes the discharge into a state with higher stability limits and maintains it there.

Control requires three key elements, namely sensors to detect deviations in the system state from the desired values, actuators to reposition the system toward the desired state, and control algorithms to convert the sensor signals to actuator commands. In the fusion plasma context, the sensors are diagnostic techniques for measuring the required aspects of the plasma state. The actuators are the means of affecting the plasma, for example, external heating, current drive and fueling systems, as well as external fields used to reconfigure the equilibrium or induce a particular plasma response. The control algorithms are essentially mathematical prescriptions, usually based on simplified (reduced) models for determining the actuator commands from diagnostic measurements.

In an AT, control of the equilibrium profiles is an essential element. This includes startup of the discharge, a steady state period, and a final shutdown. In the startup and shutdown phases, the major issue in practice is maintaining MHD stability of the plasma. In the steady state phase, the major issue is to optimize the profiles for high performance, while still avoiding MHD unstable states. Evolutionary paths to this state need to be stable at each point. Active feedback control of incipient instabilities is also essential. Active feedback stabilization of the axisymmetric (vertical) instability is routine. Typically, the plasma position (for example the current centroid) or a number of points on the plasma boundary, the iso-flux control points, are found and, if displaced from its target position or target boundary points, additional axisymmetric fields are used to reposition it (Ferron 1998, Huang 2020) by programming the currents in the external poloidal-field coils. Active stabilization of the non-axisymmetric RWM is similar in principal but requires a more complex set of sensors and applied field distribution (Liu 2000b, Liu 2004). In practice, as discussed, sufficient plasma rotation passively stabilizes the RWM but the marginal RWM

amplifies error fields which then slow the rotation, leading to destabilization of the RWM. In a reactor, active feedback stabilization of the RWM is likely required. Control of intermittent instabilities such as sawteeth and ELMs typically take the approach of either mitigating their effects or avoiding them through control of the equilibrium profiles. The other major control issue is the need to avoid and mitigate disruptions, which will be discussed in the next Section.

MHD theory provides the basis for defining the algorithms used to relate diagnostic sensor measurements to actuator controls. Typically, the algorithms use simplified models but these are often derived from full MHD predictions and are generally tested against them.

Control of MHD instabilities

Sawteeth result in a transfer of the core energy inside the $q = 1$ surface to the outside. They are normally relatively benign but if the q=1 radius is large and the core pressure high, an abnormally large amount of energy can be lost. This can happen in cases where the sawtooth period is very long, the so-called giant sawteeth, allowing a large amount of energy to build up in the core, followed by a large and fast crash that disturbs a large part of the cross section. These need to be avoided. Note that, like ELMs, sawteeth can be beneficial by periodically expelling impurities from the fusing core. Thus, means to avoid sawteeth are desirable. Alternatively, it is in many cases advantageous to control the sawtooth rate, keeping it short. Control options that have been considered involve controlling the radius of the $q = 1$ surface. Control using RF waves, particularly ECCD, ICCD has been considered to modify the current and pressure profiles around the $q = 1$ surface and tried. Another option is to run in sawtooth free regimes. This simply means controlling the profiles so that q remains well above one, avoiding completely the $1/1$ internal mode (ideal or resistive). This is the solution envisaged in the Advanced Tokamak concept.

TMs born rotating with frequency near local plasma rotation and saturate at some amplitude. But these islands slow the plasma rotation (Fitzpatrick 1991) and the plasma and mode lock. At that point, the mode generally grows rapidly as wall stabilization is lost, and disrupts the plasma. The mode typically locks in a fixed phase relationship with a pre-existing error field. Threshold scalings have been obtained from experiments and can be used to avoid low and high-density locked modes. The thresholds also depend on the pre-existing error field. These modes can be partially controlled by maintaining the plasma rotation against the natural slowing that results from the incipient instability. This entails feedback on the momentum input to the plasma.

Control of NTMs has been demonstrated (La Haye 2002) using ECCD to replace the reduced bootstrap current that results from the reduced pressure gradient inside the islands. A control scheme called 'search and suppress' has been developed whereby the island is detected and ECCD is directed using mirrors to locally be deposited in the island center. An alternative strategy under development is to modify the local current density using ECCD, essentially changing the local Δ'. This can also be modified by applying additional helical fields. For tearing modes that are destabilized by proximity to the ideal MHD β limit (Brennan 2002), the modes are linearly unstable and Δ' provides the major drive and this is the most promising strategy.

Control of the RWM follows the same strategy as the routine stabilization of the axisymmetric mode. For that case, the technique has been in use routinely since the 1970's and refined since the 1990's (Lazarus 1990, Ferron 1998, Liu 2000b, Strait 2015). The ideal instability is slowed by a resistive wall from a growth time of the order of a plasma Alfven time $\tau_A \sim 10^{-6}$ sec to the wall L/R time – the time scale for stabilizing image currents to decay. The fields are then sensed and

growing fields suppressed by applying an opposing field. In the non-axisymmetric case the major complication is the need for more sensors and actuators.

ELM control falls into four major categories usually referred to as ELM-stable, ELM-free, ELM mitigation, or ELM suppression. The first refers to plasma configurations such as QH mode or I-mode in which there are no ELMs. Control in this case is mostly concerned with maintaining the plasma operating conditions so that it stays in QH or I-mode. The second refers to plasma configurations for which the peeling-ballooning instability is suppressed for a long period. Typically, however, these are not stationary and an ELM finally appears that is larger than usual, similar to the situation with giant sawteeth. Control in this case appears to require control of the equilibrium profiles to avoid the final instability. ELM mitigation means changing conditions to replace the large Type-I ELMs by smaller, more frequent ELMs, either small Type I or Type II or Type III. Suppression, in contrast, refers to removal by full stabilization of the Type-I ELMs. ELM-free regimes however, suffer from the problem that, without ELMs, impurities and density build up in the core. ELMs do have a beneficial effect of removing core impurities, or helium ash in the case of a reactor. Mitigation solves this problem. Control of the ELM frequency in this case can be done using ELM pacing, with triggering by pellets (Lang 2004a, Baylor 2013), vertical kicks (Lang 2004b), applied non-axisymmetric fields (Canik 2010), or applied modulated non-axisymmetric fields (Solomon 2012). On the other hand, ELM suppression regimes do not result in an impurity buildup. These are obtained for certain plasma parameter regimes by applying non-axisymmetric fields (Evans 2004).

Disruption physics, prediction, prevention, and mitigation

A critical issue in tokamak experiments is the occurrence of plasma disruption, where the discharges abruptly terminate with many undesirable consequences (ITER Physics Basis Editors 1999b, Hender 2007). The causes of disruption are complicated and are not always fully understood. These can be grossly divided into MHD and non-MHD causes. We will mainly discuss the MHD causes here.[37]

As described before, there are several macroscopic MHD instabilities that can cause plasma disruption. One is the external kink mode including the resistive wall mode. The current-driven external kink becomes very dangerous when the edge safety factor (q_s for limiter plasmas and q_{95} for divertor plasmas) approaches the value of 2. The pressure-driven external kink can cause disruption when the Troyon limit is exceeded. The other important MHD cause is mode locking, which typically occurs when the $2/1$ tearing mode becomes unstable and large magnetic islands are created which (at least locally) break the plasma toroidal rotation.

A typical plasma disruption has two characteristic time scales, related to the thermal quench (TQ) and current quench (TQ). The first process, where the plasma thermal energy is rapidly lost, typically lasts a couple of milliseconds. This is a very fast process, likely involving many non-linear MHD events. The TQ is followed by the much longer CQ phase, where the plasma current resistively decays and eventually vanishes (together with the magnetic energy stored in the plasma). The time scale of the CQ depends on tokamak devices and in particular on the poloidal cross-section area (ITER Physics Basis Editors 1999b, Hender 2007).

[37] Many non-MHD causes are often directly or indirectly related to MHD events, e.g., the presence of MHD precursors, the presence of large magnetic islands in the radiative cooling model that explains the plasma density limit induced disruption (Gates 2012).

There are two important consequences associated with plasma disruption. One is the electromagnetic force acting on the conducting structures surrounding the plasma, typically the vacuum vessel and the supporting structures. This force can be large during disruption and can potentially damage the PFCs and in-vessel structures. The other critical consequence is the generation of high-energy electrons with speed close to the light speed. These so-called runaway electrons can potentially melt the PFCs, and thus must to controlled in future reactor scale devices such as ITER.

Disruption prediction and avoidance

As mentioned before, since disruption may have different origins, predicting plasma disruption is generally challenging. If a disruption is caused by MHD event, there are often magnetic precursors that can be employed, but the reliability is always an issue. Since about late 1990's, methods based on artificial intelligence (AI) have been used for the purpose of disruption prediction in tokamak experiments (Wroblewski 1997), with significant progress being made during recent years (Kates 2019). This approach requires a large operation database to train the AI algorithm (e.g., the neural network), before it can be used for predicting future experiments. Proper selection of the equilibrium input data, besides the AI architecture and the training algorithm, is critical for the success of the AI based approaches. For predicting specific classes of disruption, model-based approaches are also highly valuable. Examples are the DECAF model (Berkery 2017) based on various MHD events, and the recent initiative of the predict-first approach (Lyons 2018).

Disruption avoidance is a passive way of operating the plasma discharge. Based on *a-priori* knowledge, certain types of disruptions, in particular those involving MHD instabilities, are well known and predictable. This knowledge can be used to constrain the discharge parameters to avoid entering into the dangerous "corner". For instance, the plasma pressure can be limited to be below the Troyon limit (often following certain ℓ_i scaling curve) during the operation. The plasma current and toroidal field can be designed to avoid the edge safety factor closing to 2. The plasma toroidal rotation speed can be maintained to certain level (by various methods) to avoid locked modes. With both disruption prediction and avoidance, it is important to realize that accurate and fast equilibrium reconstruction is a critical element.

Disruption mitigation

As discussed, development of effective strategies to mitigate and control tokamak disruption is critical to reduce and avoid potential damage to the PFCs and in-vessel structures. All mitigation methods rely on rapid injection of high atomic-number Z impurities into the plasma to radiate away most of the plasma thermal energy. MHD provides a useful model to develop and test techniques to mitigate and control MHD instabilities.

A leading candidate for a disruption mitigation system (DMS) is the shattered pellet injection (SPI) approach in which a stream of cryogenic cooled pellets is injected into a bended tube and shattered into small fragments before entering into the plasma to allow higher assimilation and more rapid delivery of injected impurities than a gas injection system (Shiraki 2016, Baylor 2019). Another promising technique is the dispersive shell-pellet injection (DSPI) method in which a low-Z hollow shell filled with a dispersive payload is injected into the plasma to allow a deep penetration of impurities into the plasma core and a more effective inside-out thermal quench (Izzo 2017, Hollman 2019).

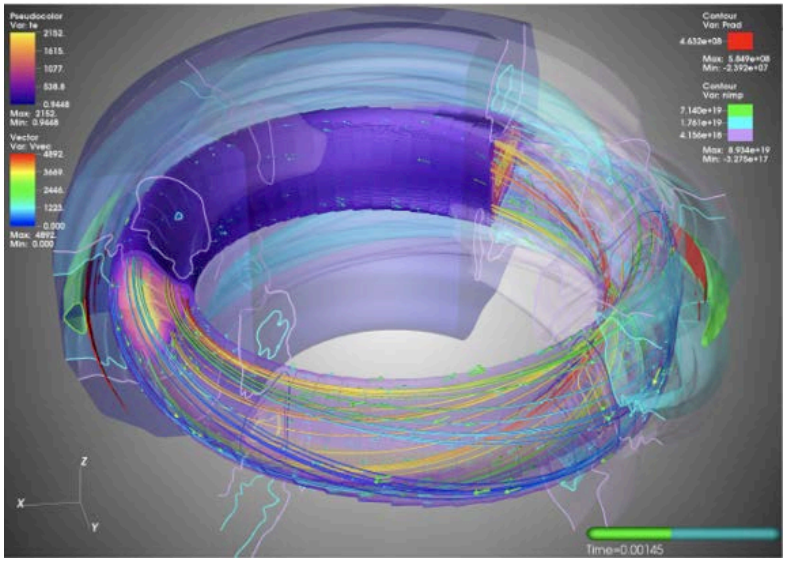

Fig. 6. NIMROD animation of a DIII-D dual-injector SPI simulation showing magnetic field lines and contours of plasma radiation and injected impurity concentration. Courtesy of C.C. Kim (Kim 2020).

An accurate disruption mitigation simulation requires integration of a global 3D MHD code with a local pellet ablation code (Kim 2019, Bosviel 2021). Progress has been made to model disruption mitigation by impurity injection and interpretation of DMS and DSPI experiments with the NIMROD (Kim 2019, Izzo 2020), M3D-C1 (Lyons 2019, Ferraro 2019) and JOREK (Hu 2018, Pamela 2020) 3D MHD codes using simplified reduced pellet ablation models. NIMROD predictions of DIII-D SPI and DSPI results are consistent with DIII-D experimental observations. An animation of a NIMROD simulation of DIII-D dual-injector SPI simulation is illustrated in Fig. 6 (Kim 2020). However, significant challenges remain to develop a robust and effective disruption mitigation technique and their simulations and validations that can address all the disruption issues, particularly regarding the generation and mitigation of runaway electrons (Boozer 2017, Lehnen 2020, Sweeney 2020).

Summary

MHD provides a useful model to describe the crucial plasma macroscopic equilibrium and stability behaviors in toroidal tokamak devices. The MHD equations provide a set of comprehensive physics constrains to understand and interpret tokamak macroscopic instabilities. Principal MHD instabilities include the internal kink modes, sawtooth, fishbone, external kink, resistive wall mode (RWM), resistive interchange, tearing and neoclassical tearing modes (NTMs), locked modes, toroidal Alfven eigenmodes (TAEs), and edge localized modes (ELMs). Predictions from MHD theory are consistent with many observed features of these instabilities. Fast-growing MHD instabilities can lead to an abrupt plasma disruption and termination that can potentially damage the device PFCs and in-vessel structures. An important MHD application is to develop robust techniques to mitigate and control instabilities. These include control of NTMs and RWMs, mitigation and suppression of ELMs, and disruption avoidance and mitigation.

Acknowledgments

The work discussed in this Chapter was supported by U.S. Department of Energy under DE-FC02-04ER54698 and DE-FG02-95ER54309.

References

Aiba N. et al. (2009). MINERVA: Ideal MHD stability code for toroidally rotating tokamak plasmas. *Comput. Phys. Comm.* 180, 1282.

Austin M.E. et al. (2019). *Phys. Rev. Lett.* 122, 115001.

Bateman G. (1978). MHD Instabilities. *MIT Press*, Cambridge.

Baylor L.R. et al. (2013). Reduction of edge localized mode intensity on DIII-D by on-demand triggering with high frequency pellet injection and implications for ITER. *Phys. Plasmas* 20, 082513. https://doi.org/10.1063/1.4818772.

Baylor L.R. et al. (2019). Shattered pellet injection technology design and characterization for disruption mitigation experiments. *Nucl. Fusion* 59, 066008. https://doi.org/10.1088/1741-4326/ab136c

Berkery J.W. et al. (2010). The role of kinetic effects, including plasma rotation and energetic particles, in resistive wall mode stability. *Phys. Plasmas* 17, 082504.

Berkery J.W. et al. (2017). A reduced resistive wall mode kinetic stability model for disruption forecasting. *Physics of Plasmas* 24, 056103.

Bernard L.C. et al. (1981). GATO: An MHD stability code for axisymmetric plasmas with internal separatrices. *Comput. Phys. Comm.* 24, 377.

Bernstein I.B. et al. (1957). An energy principle for hydromagnetic stability problems. *Proc. R. Soc. Lond. A* 244, 17. https://doi.org/10.1098/rspa.1958.0023.

Betti R. and Freiberg J.P. (1995). *Phys. Rev. Lett.* 74, 2949.

Betti R. (1998). *Phys. Plasmas* 5, 3615.

Bhattacharjee A. et al. (1983). Variational method for the three-dimensional inverse equilibrium problem in toroids. *Institute for Fusion Studies Report* IFSR 48-R. http://w3fusion.ph.utexas.edu/ifs/ifsreports/48_bhattacharjee.pdf.

Biglari H. and Chen L. (1986). *Phys. Fluids* 29, 1760.

Bogoliubov N.N. (1946). Kinetic equations. *Journal of Physics USSR* 10, 265 (1946).

Bondeson A. et al. (1992). *Phys. Fluids B* 4, 1889.

Bondeson A. and Ward D.J. (1994). *Phys. Rev. Lett.* 72, 2709.

Boozer A.H. (2005). Physics of magnetically confined plasmas. *Review of Modern Physics* 76, 1071. https://doi.org/10.1103/RevModPhys.76.1071.

Boozer A.H. (2012). Theory of tokamak disruptions. *Phys. Plasmas* 19, 058101. https://doi.org/10.1063/1.3703327.

Boozer A.H. (2017). Runaway electrons and ITER. *Nuclear Fusion* 57, 056018. https://doi.org/10.1088/1741-4326/aa6355.

Bosviel N., Parks P., and Samulyak R. (2021). Near-field models and simulations of pellet ablation in tokamaks. *Phys. Plasmas* 28, 012506. https://doi.org/10.1063/5.0029721.

Braams B.J. (1991). The interpretation of tokamak magnetic diagnostics. *Plasma Phys. Control. Fusion* 33, 715. https://doi.org/10.1088/0741-3335/33/7/001.

Brennan D.P. et al. (2002). *Phys. Plasmas*, **9**, 2998.

Burrell K.H. et al. (1987). Observation of an improved energy-confinement regime in neutral-beam-heated divertor discharges in the DIII-D tokamak *Phys. Rev. Lett.* 59, 1432. https://doi.org/10.1103/PhysRevLett.59.1432.

Burrell K.H. et al. (2001). *Phys. Plasmas* 8, 2153.

Burrell K.H. et al. (2016). Discovery of stationary operation of quiescent H-mode plasmas with net-zero neutral beam injection torque and high energy confinement on DIII-D. *Phys. Plasmas* 23, 056103.

Bussac, M.N. et al. (1975). Internal Kink Modes in Toroidal Plasmas with Circular Cross Sections. *Phys. Rev. Lett.* 35, 1638.

Cai H.S. et al. (2011). Influence of Energetic Ions on Tearing Modes. *Phys. Rev. Lett.* 106, 075002.

Canik J.M. et al. (2010). Progress in the development of ELM pace-making with non-axisymmetric magnetic perturbations in NSTX. *Nuclear Fusion* 50, 064016. https://doi.org/10.1088/0029-5515/50/6/064016

Chapman I.T. et al. (2009). Stability of the resistive wall mode in JET. *Plasma Phys. Control. Fusion* 51, 055015.

Chen L. et al. (1984).Excitation of internal kink modes by trapped energetic beam ions. *Phys. Rev. Lett.* 52, 1122. https://doi.org/10.1103/PhysRevLett.52.1122.

Chen L. (1994). *Phys. Plasmas* 1, 1519.

Cheng C.Z. and Chance M.S. (1987). NOVA: A nonvariational code for solving the MHD stability of axisymmetric toroidal plasmas. *J. Comput. Phys.* 71, 124.

Cheng C.Z. (1992). *Phys. Report* 211, 1.

Chu M.S. et al. (1995). *Phys. Plasmas* 2, 2236.

Chu M.S. and Okabayashi M. (2010). Stabilization of the external kink and the resistive wall mode. *Plasma Phys. Control. Fusion* 52, 123001.

Clauser C.F. et al. (2019). Vertical forces during vertical displacement events in an ITER plasma and the role of halo currents. *Nucl. Fusion* 59, 126037.

Colonna G. (2016). Plasma modeling: methods and applications. (*IOPscience*, IOP Publishing). https://doi.org/10.1088/978-0-7503-1200-4.

Connor J.W. et al. (1978). *Phys. Rev. Lett.* 40, 396.

Connor J.W. et al. (1988). Magnetohydrodynamic stability of tokamak edge plasmas. *Phys. Plasmas* 5, 2687.

Connor J.W. et al. (2015). *Plasma Phys. Control. Fusion* 57, 065001.

Coppi B. and Porcelli F. (1986). *Phys. Rev. Lett.* 57, 2272.

Degtyarev L. et al. (1997). The KINX ideal MHD stability code for axisymmetric plasmas with separatrix. *Comput. Phys. Comm.* 103, 10.

Dewar R.L. and Persson M. (1993). Coupled tearing modes in plasmas with differential rotation. *Phys. Fluids B* 5, 4273.

Dudson B.D. et al. (2009). BOUT++: A framework for parallel plasma fluid simulations. *Comput. Phys. Comm.* 180, 1467.

Evans T.E. et al. (2004). *Phys. Rev. Lett.* 92 235003.

Ferraro N.M. and Jardin S.C. (2009). *J. Comput. Phys.* 228, 7742.

Ferraro N.M. et. al. (2019). 3D two-temperature magnetohydrodynamic modeling of fast thermal quenches due to injected impurities in tokamaks. *Nuclear Fusion* 59, 016001. https://doi.org/10.1088/1741-4326/aae990.

Ferron J.R. et al. (1998). Real time equilibrium reconstruction for tokamak discharge control. *Nucl. Fusion* 38, 1055. https://doi.org/10.1088/0029-5515/38/7/308.

Ferron J.R. et al. (2000). Modification of high mode pedestal instabilities in the DIII-D tokamak. *Phys. Plasmas* 7, 1976. https://doi.org/10.1063/1.874053.

Finn J.M. (2006). *Phys. Plasmas* 13, 082504.

Fitzpatrick R. (1991). *Phys. Plasmas* B3, 644.

Fitzpatrick R. (1993). *Nuclear Fusion* 33, 1049.

Fitzpatrick R. (1995). *Phys. Plasmas* 2, 825.

Freidberg, J.P. (1982). Ideal magnetohydrodynamic theory of magnetic confinement systems. *Review of Modern Physics* 54, 801. https://doi.org/10.1103/RevModPhys.54.801.

Fu G.Y. and Van Dam J.W. (1989). Excitation of the toroidicity-induced shear Alfvén eigenmode by fusion alpha particles in an ignited tokamak. *Phys. Fluids B* 1, 1949.

Furth H.P. et al. (1963). *Phys. Fluids,* 6, 459.

Gates D.A. and Delgado-Aparicio L. (2012). Origin of tokamak density limit scalings. *Phys. Rev. Lett.* 108, 165004.

Glasser A.H., Greene J.M., and Johnson J.L. (1975). Resistive instabilities in general toroidal plasma configurations. *Phys. Fluids* 18, 875. https://doi.org/10.1063/1.861224.

Glasser A.H. (1997). *Los Alamos Report* LA-UR-95-528.

Glasser A.H. et al. (1999). The NIMROD Code: A New Approach to Numerical Plasma Physics. *Plasma Phys. Control. Fusion* 41, A747.

Grad H. and Rubin, H. (1956). *Proceedings of the 2nd UN Conf. on the Peaceful Uses of Atomic Energy* 31, 190. http://www-naweb.iaea.org/napc/physics/2ndgenconf/data/Proceedings 1958/NG900088.pdf.

Grad H. and Hogan J. (1970). Classical diffusion in a tokamak. *Phys. Rev. Lett.* 24, 1337. https://doi.org/10.1103/PhysRevLett.24.1337.

Graves J.P. (2004). *Phys. Rev. Lett.* 92, 185003.

Greene J.M. and Chance M.S. (1981). The second region of stability against ballooning modes. *Nucl. Fusion* 21, 453.

Grimm R.C. et al. (1976). *Meth. Comput. Phys.* 16, 253.

Gruber O., ASDEX Upgrade Project Group (1986). ASDEX Upgrade, start-up and operation. In: Knoepfel H. (eds) Tokamak Start-up. Ettore Majorana International Science Series. *Springer*, Boston. https://doi.org/10.1007/978-1-4757-1889-8_7.

Gruber R. et al. (1981). Erato stability code. *Comput. Phys. Comm.* 21, 323.

Haney S.W. et al. (1995). A fast, user-friendly code for calculating magnetohydrodynamic equilibria. *Computer in Physics* 9, 216. https://doi.org/10.1063/1.168526.

Hanson J.M. et al. (2014). Feedback-assisted extension of the tokamak operating space to low safety factor.. *Phys. Plasmas* 21, 072107. https://doi.org/10.1063/1.4886796.

Hastie R.J. et al. (2000). Effect of strong radial variation of the ion diamagnetic frequency on internal ballooning modes. *Phys. Plasmas* 7, 4561.

He Y.L. et al. (2014). Plasma-resistivity-induced strong damping of the kinetic resistive wall mode. *Phys. Rev. Lett.* 113, 175001.

Hegna C. and Bhattacharjee A. (1989). *Phys. Rev. Lett.* 63, 2056.

Hegna C.C. and Callen J.D. (1994). Stability of tearing modes in tokamak plasmas. *Phys. Plasmas* 1, 2308. https://doi.org/10.1063/1.870628.

Hender T.C. et al. (2007). Chapter 3: MHD stability, operational limits and disruptions. *Nucl. Fusion* 47, S128.

Hirshman S.P. and Jardin S.C. (1979). Two-dimensional transport of tokamak plasmas. *Phys. Fluids* 22, 731. https://doi.org/10.1063/1.862654

Hirshman S.P. and Whitson J.C. (1983). Steepest-descent moment method for three-dimensional magnetohydrodynamic equilibria. *Phys. Fluids* 26, 3553. https://doi.org/10.1063/1.864116.

Howl W., Turnbull A.D., Taylor T.S., and Lao L.L. (1992). Sensitivity of the Kink Instability to the Pressure Profile. *Phys. Fluids*, B4, 1724.

Hollmann E.M. et al. (2019). Demonstration of tokamak discharge shutdown with shell pellet payload impurity dispersal. *Phys. Rev. Lett.* 122, 065001. https://doi.org/10.1103/PhysRevLett.122.065001.

Hu B. and Betti R. (2004). *Phys. Rev. Lett.* 93, 105002.

Hu B. et al. (2006). Kinetic stability of the internal kink mode in ITER. *Phys. Plasmas* 13, 112505. https://doi.org/10.1063/1.2364147.

Hu D. et al. (2018). 3D non-linear MHD simulation of the MHD response and density increase as a result of shattered pellet injection. *Nucl. Fusion* 58, 126025. https://doi.org/10.1088/1741-4326/aae614

Huang Y. et al. (2020). GPU-optimized fast plasma equilibrium reconstruction in fine grids for real-time control and data analysis. *Nucl. Fusion* 60, 076023. https://doi.org/10.1088/1741-4326/ab91f8.

Hughes, J.W. et al. (2018). Access to pedestal pressure relevant to burning plasmas on the high field tokamak Alcator C-Mod. *Nucl. Fusion* 58, 112003.

Hunana P. et al. (2019). An introductory guide to fluid models with anisotropic temeperatures. Part 1. CGL description and collisionless fluid hierarchy. *J. Plasma Phys.* 85, 295850602. https://doi.org/10.1017/S0022377819000801.

Huysmans G.T.A. and Czarny O. (2007). MHD stability in X-point geometry: simulation of ELMs. *Nucl. Fusion* 47, 659.

Igochine V. (2015). Active control of magneto-hydrodynamic instabilities in hot plasmas. (*Springer Series on Atomic, Optical, and Plasma Physics*). https://doi.org/10.1007/978-3-662-44222-7.

ITER Physics Basis Editors et al. (1999a). Chapter 1: Overview and summary. *Nuclear Fusion* 39, 2137. https://doi.org/10.1088/0029-5515/39/12/301.

ITER Physics Basis Editors et al. (1999b). Chapter 3: MHD stability, operational limits and disruptions. *Nuclear Fusion* 39, 2251.

Ivanov A.A. et al. (2009). The SPIDER code – solution of direct and inverse problems for free boundary tokamak plasma equilibrium. *Keldysh Institute Preprints* 039. http://www.mathnet.ru/links/7d20fc4d7ffeaecab3be3dc42a0d6df1/ipmp310.pdf.

Izzo V.A. and Parks P.B. (2017). Modelng of rapid shutdown in the DIII-D tokamak by core deposition of high-Z material. *Phys. Plasmas* 24, 060705. https://doi.org/10.1088/1741-4326/ab8544

Izzo V.A. et al. (2020). Interpretative MHD modeling of dispersive shell pellet injection for rapid shutdown in tokamaks. *Nuclear Fusion* 60, 066023. https://doi.org/10.1088/1741-4326/ab8544

Jardin S.C. et al. (2020). A new explanation of the sawtooth phenomena in tokamaks. *Phys. Plasmas* 27, 032509.

Johnson J.L. et al. (1979). Numerical determination of axisymmetric toroidal magnetohydrodynamic equilibria. *J. Comput. Phys.* 32, 212. https://doi.org/10.1016/0021-9991(79)90129-3.

Kadomtsev B. B. (1975) *Sov. J. Plasma. Phys.* 1, 389.

Kamada Y. et al. (2011). Plasma regimes and research goals of JT-60SA towards ITER and DEMO. *Nuclear Fusion* 51, 073011. https://doi.org/10.1088/0029-5515/51/7/073011.

Kates-Harbeck J. et al. (2019). *Nature* 568, 526.

Kikuchi M. et al. (2019). *Nucl. Fusion* 59, 056017.

Kim C.C. et al. (2019). Shattered pellet injection simulations with NIMROD. *Physics of Plasmas* 26, 042510. https://doi.org/10.1063/1.5088814.

Kim C.C. et al. (2020). Simulations and validation of disruption mitigation and projections to ITER's disruption mitigation system. *Bulletin of the American Physical Society* CO07.00015. https://meetings.aps.org/Meeting/DPP20/Session/CO07.15.

Knolker M. et al. (2020). Optimizing the Super H-mode pedestal to improve performance and facilitate divertor integration. *Phys. Plasmas* 27, 102506.

Kramer G.J. and Fu G-Y (2006). Reversed shear Alfven eigenmodes associated with the ellipticity and triangularity Alfven gaps. *Plasma Physics and Controlled Fusion* 48, 1285. https://doi.org/10.1088/0741-3335/48/9/002.

La Haye R.J. et al. (2002). Control of neoclassical tearing modes in DIII-D *Phys. Plasmas* 9, 2051. https://doi.org/10.1063/1.1456066.

La Haye R.J. et al. (2004). Scaling of the critical plasma rotation for stabilization of the n= 1 resistive wall mode (ideal kink) in the DIII-D tokamak. *Nucl. Fusion* 44, 1197. https://doi.org/10.1088/0029-5515/44/11/005.

La Haye R.J. and Buttery R.J. (2009). The stabilizing effect of flow shear on m/n=3/2 magnetic island width in DIII-D. *Phys. Plasmas* 16, 022107.

Lang P.T. et al. (2004a). ELM pace making and mitigation by pellet injection in ASDEX Upgrade. *Nuclear Fusion* 44, 665. https://doi.org/10.1088/0029-5515/44/5/010.

Lang P.T. et al. (2004b). Frequency control of type-I ELMs by magnetic triggering in ASDEX Upgrade. *Plasma Physics and Controlled Fusion* 46, L31. https://doi.org/10.1088/0741-3335/46/11/L02

Lao L.L., Hirhman S.P., and Wieland R.M. (1981). Variational moment solutions to the Grad-Shafranov equation. *Phys. Fluids* 24, 1481. https://doi.org/10.1063/1.863562.

Lao L.L. (1984). Variational moment method for computing magnetohydrodynamic equilibria. *Computer Physics Communications* 31, 201. https://doi.org/10.1016/0010-4655(84)90045-6.

Lao L.L., St. John H.E., Stambaugh R.D. et al. (1985a). Reconstruction of current profile parameters and plasma shapes in tokamaks. *Nuclear Fusion* 25, 1611. https://doi.org/10.1088/0029-5515/25/11/007.

Lao L.L., St. John H.E., Stambaugh R.D. et al. (1985b). Separation of β_P and ℓ_i in tokamaks of non-circular cross-section. *Nuclear Fusion* 25, 1421. https://doi.org/10.1088/0029-5515/25/11/007.

Lao L.L., Greene J.M., Wang T.S., Helton F.J., and Zewadzki E.M. (1985c). Three-dimensional toroidal equilibria and stability by a variational spectral method. *Phys. Fluids* 28, 869. https://doi.org/10.1063/1.865056.

Lao L.L., Ferron J.R., Groebner R.J. et al. (1990). Equilibrium analysis of current profiles in tokamaks. *Nuclear Fusion* 30, 1035. https://doi.org/10.1088/0029-5515/30/6/006.

Lao L.L. and Jensen T.H. (1991). Magnetohydrodynamic equilibria of attached plasmas after loss of vertical stability in elongated tokamaks. *Nuclear Fusion* 31, 1909. https://doi.org/10.1088/0029-5515/31/10/009.

Lao L.L. et al. (1992). Effects of current profile on the ideal ballooning mode. *Phys. Fluids B* 4, 232. https://doi.org/10.1063/1.860438.

Lao L.L. (2000). MHD instabilities occurring near/at the transport barrier. *Plasma Physics and Controlled Fusion* 42, A51. https://doi.org/10.1088/0741-3335/42/5A/304.

Lao L.L., Kamada Y. et al. (2001). Dependence of edge stability on plasma shape and local pressure gradients in the DIII-D and JT-60U tokamaks. *Nuclear Fusion* 41, 295. https://doi.org/10.1088/0029-5515/41/3/306.

Lao L.L., St. John H.E., Peng Q. et al. (2005). MHD equilibrium reconstruction in the DIII-D tokamak. *Fusion Science and Technology* 48, 968. https://doi.org/10.13182/FST48-968.

Lazarus E.A. et al. (1990). *Nuclear Fusion* 30, 111.

Lazarus E.A. et al. (1997). Higher Fusion Power Gain with Profile Control in DIII-D Tokamak Plasmas. *Nuclear Fusion* 37, 7.

Lee G.S. et al. (1999). The design of the KSTAR tokamak. *Fusion Engineering and Design* 46, 405. https://doi.org/10.1016/S0920-3796(99)00032-0.

Lehnen M. et al. (2015). Disruptions in ITER and strategies for their control and mitigation. *Journal of Nuclear Materials* 463, 39. https://doi.org/10.1016/j.jnucmat.2014.10.075.

Lehnen M. et al. (2020). The ITER disruption mitigation strategy. *Technical Meeting on Plasma Disruptions and their Mitigation* 154. https://conferences.iaea.org/event/217/contributions/17867/.

Leonard A.W. (2014). Edge-localized-modes in tokamaks. *Physics of Plasmas* 21, 090501. https://doi.org/10.1063/1.4894742.

Levinton F.M., Zarnstorff M.C. et al. (1995). Improved confinement with reversed magnetic shear in TFTR. *Phys. Rev. Lett.* 75, 4417. https://doi.org/10.1103/PhysRevLett.75.4417.

Li L. et al. (2016). Modelling plasma response to RMP fields in ASDEX Upgrade with varying edge safety factor and triangularity. *Nucl. Fusion* 56, 126007.

Liu Y.Q. et al. (2000a). Feedback stabilization of nonaxisymmetric resistive wall modes in tokamaks. I. Electromagnetic model. *Phys. Plasmas* 7, 3681.

Liu Y.Q. and Bondeson A. (2000b). Active feedback stabilization of toroidal external modes in tokamaks. *Phys. Rev. Lett.* 84, 907.

Liu Y.Q. et al. (2004). Stabilization of resistive wall modes in ITER by active feedback and toroidal rotation. *Nucl. Fusion* 44, 232.

Liu Y.Q. et al. (2008). Toroidal self-consistent modeling of drift kinetic effects on the resistive wall mode. *Phys. Plasmas* 15, 112503.

Liu Y.Q. et al. (2009). An improved method to evaluate the ideal no-wall beta limit from resonant field amplification measurements in JET. *Plasma Phys. Control. Fusion* 51, 115005.

Liu Y.Q. (2010). Effects of α particles on the resistive wall mode stability in ITER. *Nucl. Fusion* 50, 095008.

Liu Y.Q. (2011). Modelling of plasma response to resonant magnetic perturbation fields in MAST and ITER. *Nucl. Fusion* 51, 083002.

Liu Y.Q. et al. (2012). Modification of Δ′ by magnetic feedback and kinetic effects. *Phys. Plasmas* 19, 092510.

Liu Y.Q. et al. (2013). Toroidal modeling of penetration of the resonant magnetic perturbation field. *Phys. Plasmas* 20, 042503.

Liu Y.Q. et al. (2016). ELM control with RMP: plasma response models and the role of edge peeling response. *Plasma Phys. Control. Fusion* 58, 114005.

Liu Y.Q. et al. (2019). MARS-F modeling of post-disruption runaway beam loss by magnetohydrodynamic instabilities in DIII-D. *Nucl. Fusion* 59, 126021.

Lutjens H. et al. (2001). *Plasma Phys. Control. Fusion* 43, A339.

Luxon J.L. (2002). A design retrospective of the DIII-D tokamak. *Nuclear Fusion* 42, 614. https://doi.org/10.1088/0029-5515/42/5/313.

Lyons B.C. et al. (2018). Predict-first experimental analysis using automated and integrated magnetohydrodynamic modeling. *Phys. Plasmas* 25, 056111.

Lyons B.C. et al. (2019). Axisymmetric benchmarks of impurity dynamics in extended-magnetohydrodynamic simulations. *Plasma Physics and Controlled Fusion* 61, 064001. https://doi.org/10.1088/1361-6587/ab0e42.

Medvedev S.Y. et al. (2015). *Nucl. Fusion* 55, 063013.

Meneghini O. et al. (2016). Integrated fusion sinulations with self-consistent core-pedestal coupling. *Phys. Plasmas* 23, 4947204. http://dx.doi.org/10.1063/1.4947204.

Mercier C. (1960). A necessary condition for hydromagnetic stability of plasma with axial symmetry. *Nucl. Fusion* 1, 47. https://doi.org/10.1088/0029-5515/1/1/004.

Mercier C. (1962). *Nucl. Fusion Suppl. Pt.* 2, 801.

Militello F. et al. (2004). Effects of local features of the equilibrium current density profile on linear tearing modes. *Phys. Plasmas* 11, 125. https://doi.org/10.1063/1.1632495.

Mikhailovskii A.B. et al. (1997). *Plasma Phys. Rep.* 23, 844.

Moret J.-M. et al. (2015). Tokamak equilibrium reconstruction code LIUQE and its real time implementation. *Fusion Eng. Des.* 91, 1. https://doi.org/10.1016/j.fusengdes.2014.09.019.

Northrop T.G. (1963). The Adiabatic Motion of Charged Particles. (*Interscience*. New York).

Pamela S.J.P. et al. (2020). Extended full-MHD simulation of non-linear instabilities in tokamak plasmas. *Phys. Plasmas* 27, 102510. https://doi.org/10.1063/5.0018208.

Park W. et al. (1999). *Phys. Plasmas* 6, 1796.

Paz-Soldan et al. (2015). *Phys. Rev. Lett.* 114, 10500100Porcelli F. (1991). Fast particle stabilization. *Plasma Phys. Control. Fusion* 33, 1601. https://doi.org/10.1088/0741-3335/33/13/009.

Piovesan P. et al. (2014). Tokamak Operation with Safety Factor q_{95}<2 via Control of MHD Stability. *Phys. Rev. Lett.* 113, 045003.

Politzer P.A. et al. (2008). Influence of toroidal rotation on transport and stability in hybrid scenario plasmas in DIII-D. *Nucl. Fusion* 48, 075001. https://doi.org/10.1088/0029-5515/48/7/075001.

Porcelli F. et al. (1996). Model for the sawtooth period and amplitude. *Plasma Phys. Control. Fusion* 38, 2163.

Qu W.X. and Callen J.D. (1985). *University of Wisconsin* report UWPR 85-5.

Rampp M. et al. (2017). A parallel Grad-Shafranov solver for real-time control of tokamak plasmas. *Fusion Science and Technology* 62, 409. https://doi.org/10.13182/FST12-481.

Reimerdes H. et al. (2004). Measurement of the resistive-wall-mode stability in a rotating plasma using active MHD spectroscopy. *Phys. Rev. Lett.* 93, 135002. https://doi.org/10.1103/PhysRevLett.93.135002.

Reimerdes H. et al. (2007). *Phys. Rev. Lett.* 98, 055001.

Ren J. et al. (2016). A comparative study of ideal kink stability in two reactor-relevant tokamak plasma configurations with negative and positive triangularity. *Plasma Phys. Control. Fusion* 58, 115009.

Ren Q. et al. (2011). High spatial resolution equilibrium reconstruction. *Plasma Phys. Control. Fusion* 53, 095009. https://doi.org/10.1088/0741-3335/53/9/095009.

Rogers B.N. and J.F. Drake (1999). Diamagnetic stabilization of ideal ballooning modes in the edge pedestal. *Phys. Plasmas* 6, 2797.

Ryan D. et al. (2015). Toroidal modelling of resonant magnetic perturbations response in ASDEX-Upgrade: coupling between field pitch aligned response and kink amplification. *Plasma Phys. Control. Fusion* 57, 095008.

Sabbagh S.A. et al. (2006). *Nucl. Fusion* 46, 635.

Shafranov V.D. (1958). *Sov. Phys. JETP* 6, 545. http://www-naweb.iaea.org/napc/physics/2ndgenconf/data/Proceedings 1958/NG900088.pdf.

Shafranov V.D. (1970). Sov. *Phys. Tech. Phys.* 15, 175.

Shiraki D. et al. (2016). Thermal quench mitigation and current quench control by injection of mixed species shattered pellets in DIII-D. *Phys. Plasmas* 23, 062516. https://doi.org/10.1063/1.4954389.

Snipes J.A. et al. (1998). *Plasma Phys. Control. Fusion* 40, 765.

Snyder P.B. et al. (2002). Edge localized modes and the pedestal: A model based on coupled peeling–ballooning modes. *Phys. Plasmas* 9, 2037.

Snyder P.B. et al. (2007). Stability and dynamics of the edge pedestal in the low collisionality regime: physics mechanisms for steady-state ELM-free operation. *Nucl. Fusion* 47, 961.

Snyder P.B. et al. (2009). Development and validation of a predictive model for the pedestal height. *Phys. Plasmas* 16, 056118.

Snyder P.B. et al. (2011). A first-principles predictive model of the pedestal height and width: development, testing and ITER optimization with the EPED model. *Nucl. Fusion* 51, 103016.

Snyder P.B. et al. (2015). Super H-mode: theoretical prediction and initial observations of a new high performance regime for tokamak operation. *Nucl. Fusion* 55, 083026.

Snyder P.B. et al. (2019). High fusion performance in Super H-Mode experiments on Alcator C-Mod and DIII-D. *Nucl. Fusion* 59, 088017.

Solomon W.M. et al. (2012). ELM pacing using modulated non-axisymmetric magnetic field on DIII-D. *Nucl. Fusion* 52, 033007. https://doi.org/10.1088/0029-5515/52/3/033007.

Solomon W.M. et al. (2013). Access to high beta advanced inductive plasmas at low injected torque. *Nucl. Fusion* 53, 093033. https://doi.org/10.1088/0029-5515/53/9/093033.

Solomon W.M., Snyder P.B. et al. (2014). Access to a new plasma edge state with high density and pressures using the quiescent H mode. *Phys. Rev. Lett.* 113, 135001. https://doi.org/10.1103/PhysRevLett.113.135001.

Solomon W.M., Snyder P.B. et al. (2016). Exploration of the super H-mode regime on DIII-D and potential advantages for burning plasma devices. *Phys. Plasmas* 23, 056105. https://doi.org/10.1063/1.4944822.

Solovev L.S. (1968). *Sov. Phys. JETP* 26, 400.

Sovinec C.R. et al. (2004). Nonlinear Magnetohydrodynamics Simulation Using High-order Finite Elements. *J. Comput. Phys.* 195, 355.

Srinivasan et al. (2010). *Plasma Phys. Control. Fusion* 52, 035007.

Stambaugh R.D. et al. (1984). Test of beta limits as a function of plasma shape in Doublet III. *Plasma Physics and Controlled Nuclear Fusion Research* Vol. I, 117. http://www-naweb.iaea.org/napc/physics/FEC/STIPUB670_VOL1.pdf.

Strait E.J.. (1994a). Stability of high beta tokamak plasmas. *Phys. Plasmas* 1, 1415. https://doi.org/10.1063/1.870691.

Strait E.J. et al., (1994b). *Proc. 20th Eur. Conf. on Controlled Fusion and Plasma Physics* (Lisbon, 1993) vol 1 (Petit-Lancy: European Physical Society) p 211.

Strait E.J., Lao L.L. et al. (1995). Enhanced confinement and stability in DIII-D discharges with reversed magnetic shear. *Phys. Rev. Lett.* 75, 4421. https://doi.org/10.1103/PhysRevLett.75.4421.

Strait E.J.. (2015). Magnetic control of magnetohydrodynamic instabilities in tokamaks. *Phys. Plasmas* 22, 021803. https://doi.org/10.1063/1.4902126.

Sweeney R. et al. (2020). MHD stability and disruption in the SPARC tokamak. *J. Plasma Phys.* 86, 865860507. https://doi.org/10.1017/S0022377820001129.

Takeda Tatsuoki and Tokuda Shinji (1991). Computation of MHD equilibrium of tokamak plasma. *J. Comput. Phys.* 93, 1. https://doi.org/10.1016/0021-9991(91)90074-U.

Tokuda S. and Watanabe T. (1999). *Phys. Plasmas* 6, 3012.

Troyon F. et al. (1984). *Plasma Phys. Control. Fusion* 26, 209.

Turnbull A.D. et al. (1986). Beta Limits in H--Mode Like Discharges. *J. Comp. Phys.* 66, 391.

Turnbull A.D. and Troyon F.S. (1989) Toroidal Effects on Current Driven Modes in Tokamaks. *Nucl. Fusion*, 29, 1887.

Turnbull A.D. et al. (1993). Global Alfvén Modes: Theory and Experiment. *Phys. Fluids* B5, 2546.

Turnbull A.D. et al. (2002). *Nucl. Fusion* 42, 917.

Turnbull A.D. et al. (2005). *Fusion Sci. Tech.* 48, 875.

Turnbull A.D. et al. (2016) The external kink mode in diverted tokamaks. *J. Plasma Phys.* 82, 515820301.

Wagner F. (2007). A quarter-century of H-mode studies. *Plasma Physics and Controlled Fusion* 49, B1. https://doi.org/10.1088/0741-3335/49/12B/S01.

Wahlberg C. and Bondeson A. (2000). *Phys. Plasmas* 7, 923.

Wan Y., Li. J., Weng P. and EAST Team (2006). First engineering commissioning of EAST tokamak. *Plasma Science and Technology* 8, 253. https://doi.org/10.1088/1009-0630/8/3/01.

Wang Z.R. et al. (2015). Three-Dimensional Drift Kinetic Response of High-β Plasmas in the DIII-D Tokamak. *Phys. Rev. Lett.* 114, 145005.

Webster A.J. and Gimblett C.G. (2009). *Phys. Rev. Lett.* 102, 035003.

Wesson J.A. (1978). *Nucl. Fusion* 18, 87.

Whyte D. et al. (2010). *Nucl. Fusion* 50, 105005.

Wilson H.R. et al. (1996). *Plasma Phys. Control. Fusion* 38, A149.

Wilson H.R. et al. (2002). *Phys. Plasmas* 9, 1277.

Wong K. et al. (2000). Internal kink instability during off-axis electron cyclotron current drive in the DIII-D tokamak. *Phys. Rev. Lett.* 85, 996.

Wroblewski D. et al. (1997). Tokamak disruption alarm based on a neural network model of the high- beta limit. *Nucl. Fusion* 37, 725.

Wu T.T. et al. (2018). Toroidal modelling of resistive internal kink and fishbone instabilities. *Phys. Plasmas* 25, 052054.

Wu T.T. et al. (2019). Toroidal shear flow and thermal particle drift kinetic effects on internal kink mode. *Phys. Plasmas* 26, 102102.

Xia G.L. et al. (2019). Effects of poloidal and parallel flows on resistive wall mode instability in toroidally rotating plasmas. *Nucl. Fusion* 59, 126035.

Xu X.Q. and Cohen R.H. (1998). *Contrib. Plasma Phys.* 36, 158.

Yang X. et al. (2016). *Plasma Phys. Control. Fusion* 58, 114006.

Zheng L.-J. and Kotschenreuther M. (2006). *J. Comput. Phys.* 211, 748.

Zheng L.-J. *et al*. (2010). *J. Comput. Phys.* 229, 3605.

Zohm H. et al. (1995). *Nucl. Fusion* 35, 543.